Theoretical investigation of self-trapped hole (STH) polarons in cubic and rhombohedral phases of NaNbO3

Auteur : Agharezaei, Parastoo
Promoteur(s) : Ghosez, Philippe; 10904
Faculté : Faculté des Sciences
Diplôme : Master en sciences physiques, à finalité approfondie
Année académique : 2019-2020
URI/URL : http://hdl.handle.net/2268.2/9972

2.4172.118 2.321

Theoretical investigation of self-trapped hole (STH) polarons in cubic ($Pm\bar{3}m$) and rhombohedral ($R\bar{3}$) phases of $NaNbO_3$

Parastoo Agharezaei

Under supervision of
Pr. Karsten Albe
Pr. Philippe Ghosez

Committee members
Pr. Peter Schlagheck
Dr. Eric Bousquet
Dr. Stéphane Dorbolo

This thesis is submitted for obtaining the Master's double diploma of Functionalized Advanced Materials and Engineering (FAME+)

Université de Liège, Technische universität darmstadt
August 2020

Abstract

In this study we investigate the formation of the self-trapped hole (STH) in two high and low-temperature phases of $NaNbO_3$ (cubic and rhombohedral phases) by using both DFT with application of local potentials and HSE06. In both phases, we first investigate the existence of polaron in the lattice which is manually distorted and one electron is removed from its system. Then various energy regimes of formed STH is calculated using DFT+U and HSE06 in order to investigate the stability of the formed STH. Comparing trapping energy of STH in rhombohedral and cubic phase shows that the appeared STH in rhombohedral phase of $NaNbO_3$ is noticeably more stable compared to the one in cubic phase in condition which U parameter applied on Nb and O atoms in both cases are equal. It is then shown that applying various U parameters on Nb and O atoms, yield a piecewise linear behaviour of the total energy with respect to fractional charge. In order to find the best U parameter which can be used for future works, lattice parameters and band gap obtained from different composition of U parameter on Nb and O are compared to the available experimental results. In the case of rhombohedral phase, U(Nb4d)= 4,6 eV and U(O2p)= 4 eV gives a very good linear response in total energy curves with respect to fractional charge and have a good agreement with experimental data. For cubic phase, U(Nb4d)= 4 eV and U(O2p)= 6 eV is in best agreement with experimental studies.

Contents

List of Figures

List of Tables

Chapter 1

Introduction

In polarised materials, with partial ionic properties, the charges can be localized to a special site and form a polaron [1, 2]. Depending on the size of distortion that polaron cause in the system it is categorized into small (Holstein polaron) and large (Fröhlich) polaron [3]. The polaron transport mechanism unlike free charges in simple metals, is by a hopping mechanism which is a thermally activated process and it is exponentially dependent on temperature [4, 5]. Unlike typical semiconductors, the energy barrier for motion of polarons is not the band gap energy but it is the energy difference between the conduction band minimum (CBM) and polaronic band state which will be smaller compared to energy gap [5]. However, since polaron transport mechanism is dependent on temperature, their mobility is not high and it is extremely disadvantageous for materials application [6]. Therefore, investigation of appearance of polaron in different materials is of great importance as it directly affects its properties. Formation of polarons in transition metal oxides is favorable due to strong phonon-electron interactions.

$NaNbO_3$ is a transition metal oxide with perovskite structure which has attracted widespread attention as it is environmental friendly, non-toxic, low cost, low density and shows outstanding chemical, physical, mechanical and electronic properties which makes it a good candidate for various technological applications [7–10]. $NaNbO_3$ goes through a very complex sequence of phase transitions in different temperatures [11, 12]. Different high and low temperature phases of this material has been studied both experimentally and theoretically [13, 14]. Although, there is not much debate on high temperature phases of $NaNbO_3$ among researchers, there is strong controversies regarding low and room temperature phases of $NaNbO_3$ [13,14]. $NaNbO_3$ has a cubic ($Pm\bar{3}m$) crystal structure and paraelectric properties in temperatures above 913 k. At low temperatures below 173 K, $NaNbO_3$ has a rhombohedral crystal system with space group $R3c/R\bar{3}$ and ferroelectric (FE) properties. It is widely accepted that in a wide range of low temperatures, there is co-existence of both rhombohedral and orthorhomic phases [11, 12].

Since formation of polarons directly affects different properties of $NaNbO_3$ such as electronic and optoelectronic properties, studying the appearance of polaron in this perovskite material can be very beneficial to its application in electronics and

photocatalysis [15–17]. The formation of a small polaron which is bound to a defect inside the lattice structure in various perovskites including $NaNbO_3$ is already studied [8, 18, 19]. However, the self-trapped hole/electron polarons are harder to detect and not enough information is available in this subject. There has been studies which have detected the small polarons in different similar perovskite materials such as $BaTiO_3$, and $SrTiO_3$, which provided the motivation for the present research [6]. We investigate the formation of STH polarons in cubic and rhombohedral phases of $NaNbO_3$ by using two different functionals of DFT+U and hybrid functionals (HSE06). Since exploring the polaronic effect is highly sensitive to the method that has been used, results from these two functional are compared. The stability of the polarons in two phases are investigated by comparing their different energy regimes. The optimum values of U parameter on both Nb and O are investigated using piecewise linearity method.

Chapter 2

Theory

2.1 Physics of Polaron

Polarons have attracted a great attention during the last 50 years. There has been both theoretical and experimental studies of polaron properties. Polarons form in polar crystals namely as ionic crystal and polar semiconductors [20].

Electron/hole transport inside a material directly affects its electronic properties. An electron can be a free charge in a fermi gas or it can be localized to the atoms in its surrounding. Neglecting forces between conduction electrons (or free charge carriers) with ions in the material, is no more valid and electron-ion Coulombic forces need to be considered [5, 20]. Depending on the type of material which is under study, there are three types of interaction between a charge carrier and lattice [20]:

- Fröhlich coupling: This type of interaction occurs in polar crystals where charge carrier strongly couples with Longitudinal Optical (LO) phonons.
- Piezoelectric coupling: In materials with a specific symmetry, charge carrier couples with acoustic phonons which is addressed as piezoelectric coupling.
- Deformation coupling: In all type of crystal structures, electron energy can be affected by the deformation in the system. This deformation is caused due to acoustic phonons.

Fröhlich coupling is a strong coupling and the focus of this study. This mechanism can cause the formation of polarons in the system. When there is a free charge carrier in the lattice structure, it polarizes the atoms in its neighborhood and move them from their original position. This adds an additional potential well around subjected charge carrier and free charge becomes bound to the distorted site. This local distortion and polarization formed in the system, move along when the charge start moving under an electric field. This charge carrier and its associated local distortion and polarization is referred to as polaron. If the localization of charge carrier to a distorted site has higher gain in energy compared to the energy required to move the atoms from their equilibrium sites, a stable polaron can form [2, 20, 21].

Polaron has different effective mass compared to the free charge that initially caused its formation. Formation of polarons in Transition metal oxides (TMO) have been widely investigated due to their various technological applications in photovoltaics, thermoelectrics, transistors, sensors, and more [22–25]. Therefore, studying charge transport and electron-phonon coupling is of great importance and electronic properties of TMOs can be improved by energy barrier engineering.

The associated distortion in the system in compounds with strong phonon-electron/ hole coupling is small and limited to the unit cell. In these cases, where there is small distortion compared to the lattice parameters, small polarons (Holstein polaron) is formed [5, 26]. Fig.2.1.a shows a small polaron in TMO lattice. In the case of Holstein polaron, electron-phonon coupling is strong which restricts the formed distortion to its neighborhood. When distortion caused by the trapped charge carrier is large compared to unit cell parameters, large polarons (Fröhlich polaron) form [5, 27]. In such case, phonon-electron interaction is weaker, long range interactions become noticeable and distortion caused by the charge carrier is spatially extended [5, 27].

2.1.1 Polarons in ionic crystals

In ionic crystals, there is a strong coupling between the charge carrier and lattice (Fröhlich coupling) which forms a dielectric medium [2, 21]. Charge carrier in the polar ionic crystal, induce a displacement field [28]:

$$D(r, r_{el}) = -\nabla \frac{e}{|r - r_{el}|} \tag{2.1}$$

Where D is the displacement field caused by the charge carrier, e is electric charge value, r is the spatial coordinate and r_{el} is the position of the charge carrier. Coupling of this displacement field with lattice phonons (lattice dynamics in general) forms a Polarization field [28]:

$$P(r) = \frac{1}{4\pi} \nabla V_{pol} \tag{2.2}$$

Where $P(r)$ is polarization field at position r and V_{pol} is polarization potential. In order to investigate polarons in the material, we need to define a frequency dependent dielectric constant [28]:

$$D = \varepsilon(\omega) E \tag{2.3}$$

Where ε is dielectric constant, ω is frequency and E is the electric field inside dielectric medium. It is worth mentioning that dielectric constant is only dependent on frequency while equation 2.3 shows that the produced electric field is dependent on dielectric constant. Displacement field, polarization field and electric field are related given equation 2.5 [28]:

$$4\pi P(r) = D(r) - E(r) \tag{2.4}$$

The response to the produced electric field in dielectric medium has two contributions:

(i) High frequency contribution: This type of contribution is produced by high frequency oscillations of electron clouds around atomic positions.

(ii) Low frequency contributions: Oscillation of positive and negative ions cause a low frequency contribution.

Polarization field can then be written as [28]:

$$P(r) = P_0(r) + P_\infty(r) \tag{2.5}$$

Where $P_0(r)$ and $P_\infty(r)$ are polarization field caused by low frequency and high frequency contributions, respectively. Low frequency contribution to the polarization field is roughly independent from high frequency perturbations which is an important assumption for investigation of polarons.

In order to understand the nature of polarons, a dielectric continuous medium is considered. A charge carrier with velocity υ is constrained to a small volume with radius R_1. The characteristic time for ions oscillations is $\frac{2\pi}{\omega_0}$. The motion of charge carrier can be static or dynamic. Both cases will be discussed. Charge carrier motion is assumed to be static if it is further away from $\frac{2\pi}{\omega_0}\upsilon$ (outside the sphere) while its motion is dynamic inside the sphere with constant potential [2, 21, 28] The potential energies of charge carrier in and out of the imaginary volume (with radius R_1) are defined as:

(i) Inside the imaginary sphere [28]:

$$E_{pot} = \frac{-e^2}{\tilde{\varepsilon} R_1} \tag{2.6}$$

(ii) Outside the imaginary sphere [28]:

$$E_{pot} = \frac{-e^2}{\tilde{\varepsilon} r} \tag{2.7}$$

If we minimize the total energy with respect to R_1, considering static motion of electron [28]:

$$R_1 = \frac{(2\pi\hbar)^2 \tilde{\varepsilon}}{me^2} \tag{2.8}$$

Investigation of polaron in a dynamic fashion, where characteristic wavelength of electron is smaller than $\frac{2\pi}{\omega_0}\upsilon$, radius of trapping potential is obtained [28]:

$$R_1 = 2\pi(\frac{\hbar}{m\omega_0})^{\frac{1}{2}} \tag{2.9}$$

The potential energies for static and dynamic motion of electron are related to each other by equation 2.10 [28]:

$$-\frac{U_1}{\hbar\omega_0} = (\frac{U_2}{\hbar\omega_0})^2 = \frac{1}{2\pi^2}{\alpha_F}_r^2 \tag{2.10}$$

Where U_1 and U_2 corresponds to potential energies of electron in static and dynamic fashion, respectively. α_{Fr} is a dimensionless coupling constant defined by Fröhlich as [2, 21, 28]:

$$\alpha_{Fr} = \frac{e^2}{\tilde{\varepsilon}\sqrt{2}} \sqrt{\frac{m}{\hbar^3 \omega_0}} \tag{2.11}$$

α_{Fr} can vary between 0.1-5, depending on the type of material. Large values of α_{Fr} refers to the static motion of charge carrier and small values correspond to the dynamic motion [28].

2.2 Polaron transport in solids

Electron transport in a system can be categorized into two cases:

- Free electron/hole which is the typical behavior of simple metals,
- Electrons/holes which are localized inside a defective site of the lattice (distortion or vacancy).

Second scenario will be discussed with more details in this section. The idea that a self-trapped charge can be formed was initially proposed by Landau [2]. As it is already discussed in the previous section, trapping of the hole is restriction of charge to a quite deep potential well in a specific site which it can no more move freely and cause the formation of a distortion inside the lattice structure. The polaron transport mechanism can change electrical conductivity behavior of the material and it transfers by a hopping mechanism. In materials which the mobility of charges are dominated by a hopping mechanism, since the charge carrier needs energy to overcome the band gap and this can be provided by thermal energy, the conductivity is an Arrhenius-type temperature dependent [4,5]. In normal semiconductors (band semi-conductors), the charge carriers need an energy equal to their band gap energy in order to be activated. In materials where polarons form, the activation energy is the energy difference between local band state of polaron and the conduction band [29, 30]. Fig. 2.1.a schematically shows how the polaron is formed inside the lattice structure of a TMO. As it can be seen in the image, localization of negative charge to one of the cations caused a distortion in that site which as a result, O atoms are moving further away and cations are moving closer to the center. Fig. 2.1.b shows the hopping mechanism of a small polaron in a TMO moving from one site to a neighbouring site. As polaron moves along the bond length, it needs to overcome an energy barrier (W_H) which is shown in Fig. 2.1.c. The deformation in Fig. 2.1.c is equal and reversible in both sites, consequently, the hopping mechanism indicated in Fig. 2.1.c is adiabatic and the energy barrier for transport of polaron from the atom on the right to the atom in the left is equal to the energy barrier for a case which the opposite occurs.

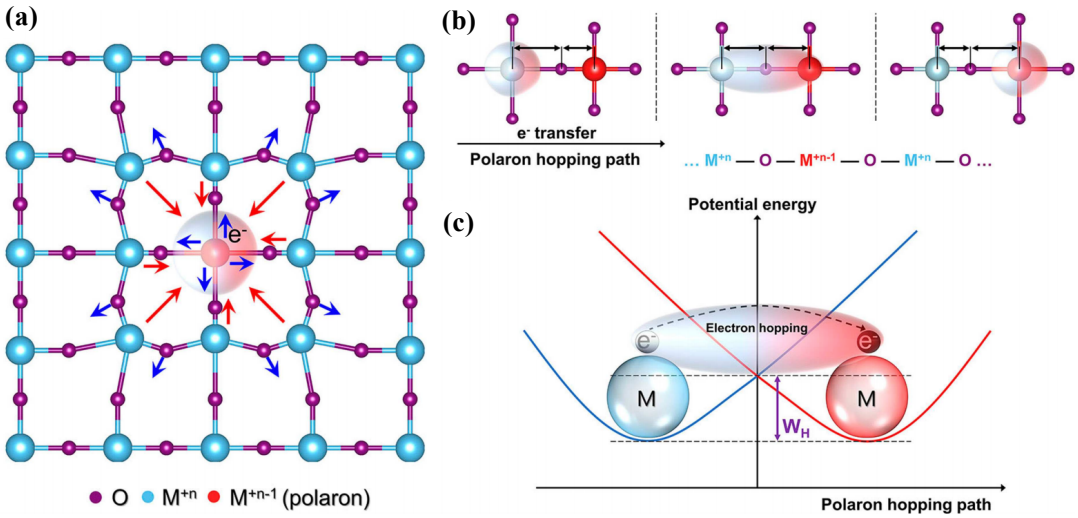

Figure 2.1: (a) Schematic illustration of polaron formation with its associated lattice distortion, (b) Change of bond length during polaron hopping mechanism, (c) Energy diagram illustration for electron moving from one lattice site to its neighbour site [5].

Fig. 2.2 shows the formation of polaron in cubic phase of $SrTiO_3$. Erhart. et al [6]. shows that STH in $SrTiO_3$ is formed on 2p orbital of an O atom. As it can be seen in Fig. 2.2.a, all the other O atoms are moving closer to the one with major positive charge localization while cations (Sr and Ti) are moving further away from the O atom in the center. Fig. 2.2.b clearly shows the charge localization with a 2p nature on the O in the center.

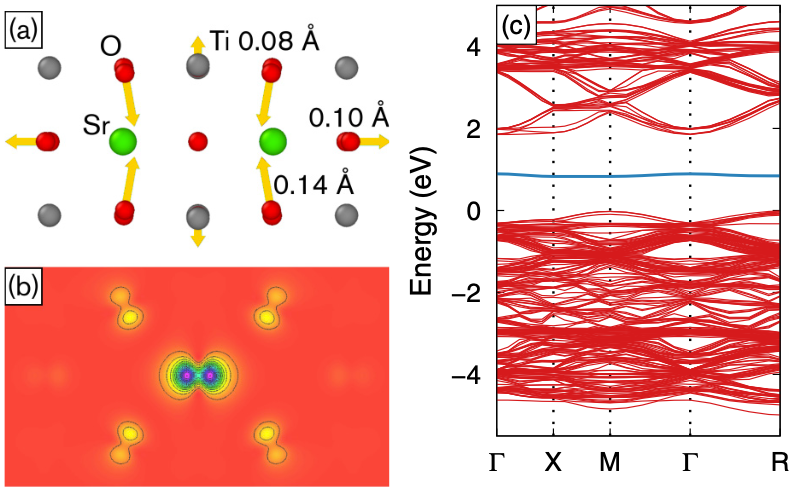

Figure 2.2: Polaron formation in cubic phase of $SrTiO_3$; (a) geometric illustration of formed distortion in the polaronic site, (b) partial charge density on each atom in the polaronic site (c) band structure of cubic phase of $SrTiO_3$ showing a STH band level [6].

Fig. 2.3 shows the band diagram of a material with polaron, schematically. The activation energy barrier for a charge is sum of:

- J: Electron transfer integral,
- E_S: Energy required for generation of a charge carrier,
- W_H: Hopping energy barrier.

While E_S and W_H are determined by thermal activation process which is discussed in this section, J is determined by overlap between wavefunction of neighbouring sites [5]. These different energy regimes are shown in Fig. 2.3.

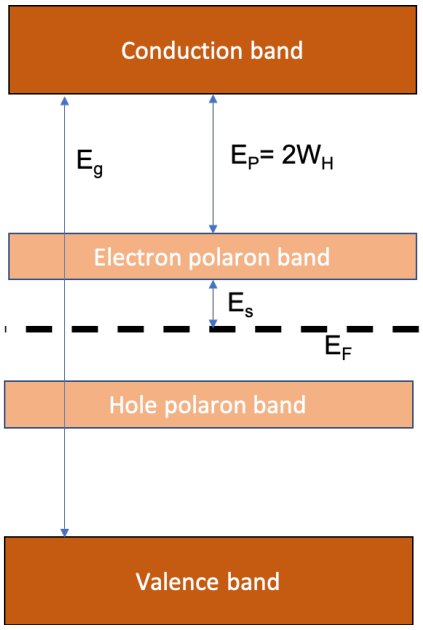

Figure 2.3: Schematic illustration of band diagram in materials with localized charge carriers [5].

2.3 Review on formation of polarons in oxides

As it is discussed earlier, the formation of polaron is along with the change in the oxidation state of atoms and a distortion in the lattice. DFT calculations overdelocalizes the charge in the system, while for obtaining a polaronic state in the system, charge needs to be localized. Geneste et al. investigated the formation of both STH polarons and oxygen-type hole polarons in $BaSnO_3$ using modified Hubbard model (DFT+U) and occupation matrix control. The reported formation energy of STH polaron in $BaSnO_3$ is 0.20 eV while oxygen-type hole polarons has a formation energy of -0.3 eV. Deskins et al. has shown that in TiO_2 with oxygen vacancies, applying a Hubbard U-parameter on the O(2p) states can change the oxidation state of Ti^{4+} to Ti^{3+} by adding one electron to the system. Ding et al. showed that introducing a Li atom into the MoO_3 cell, can change the oxidation state of Mo^6+ to Mo^5+. In both TiO_2 and MoO_3, the lattice structure is distorted. Erhart et al. also reported the formation of STH polarons in $SrTiO_3$ and $BaTiO_3$ by using DFT+U

and hybrid functional. The obtained formation energy of STH polaron in $SrTiO_3$ using DFT+U (U parameter of 8 eV on O(2p) states) and HSE06 is -0.09 eV. The formation energy of polarons in $BaTiO_3$, reported by Erhart et al. is -0.20 eV with application of DFT+U and hybrid functional. the formation energy of STH polaron in $PbTiO_3$ reported by Erhart et al is +0.24 eV (using LDA+U) which implies that STH polarons does not form in this perovskite oxide. The reason for metastable polaronic state in $PbTiO_3$ can be attributed to the strong coupling between Pb(6s) and O(2p) orbitals. This strong coupling puts VBM of $PbTiO_3$ in higher energy levels compared to $BaTiO_3$ and $SrTiO_3$.

2.4 $NaNbO_3$ ($NaNbO_3$)

2.4.1 Phase Transitions in $NaNbO_3$

Sodium Niobate with chemical formula ($NaNbO_3$) is among some of the most attractive materials due to its application in wide range of optics, optoelectronics, thermoelectrics, sensors, and photocatalysis. $NaNbO_3$ is a ferroelectric (at room temperature) perovskite material which similar to other perovskite structures, it goes through several phase transitions [12, 31]. The perovskite structure of $NaNbO_3$ consists of NaO_6 octahedras with Na atoms in between them (shown in Fig. $NaNbO_3$fig:phases of $NaNbO_3$. Both phase transitions in high and low temperatures are due to tilting of NaO_6 octahedra [12, 13]. Due to $NaNbO_3$ appealing electronic and mechanical properties, it is a good option for technological applications.

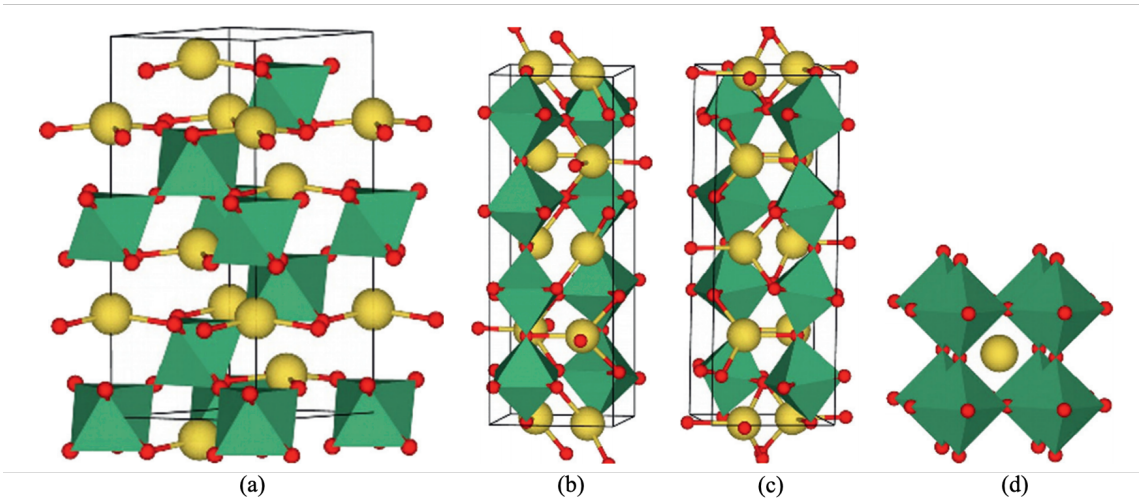

Figure 2.4: Schematic illustration of different crystal systems of $NaNbO_3$*; (a) The rhombohedral R3c phase, (b) the orthorhombic Pbcm phase, (c) monoclinic Pm phase, and (d) cubic* $Pm\bar{3}m$ *phase [12].*

Table $NaNbO_3$tab:phase-transitions-in-$NaNbO_3$hows that $NaNbO_3$ has an AFE properties in room temperature (below 633 K). $NaNbO_3$ has a cubic structure with space group of $Pm\bar{3}m$ with paraelectric properties (PE) at temperatures higher

than 913 K [12]. At 913 K the crystal structure changes to tetragonal system with $P4/mbm$ space group. By decreasing the temperature to 633 K, $NaNbO_3$ goes through several phase transitions, having orthorhombic crystal structure while it shows antiferroelectric (AFE) behavior in temperature range of 633-753 K. $NaNbO_3$ has ferroelectric (FE) properties in temperatures lower than room temperature. There is not much debate on high-temperature phases of $NaNbO_3$ while researches do not completely agree on low-temperature phases of this material [12,32]. Although, there are plenty of studies available on experimental investigation of $NaNbO_3$ phase transitions in low-temperatures, there are several controversies regarding FE behavior of $NaNbO_3$ in low temperatures. Data obtained from X-ray and neutron powder diffraction shows that it has a mixture of monoclinic Pm phase to Orthorhombic crystal structure with $Pbcm$ space group at room temperature. Experimental studies also reveal that $NaNbO_3$ shows both FE ($R3c$ phase) and AFE ($Pbcm$) behavior in a wide range of temperatures as these phases have a very small energy difference. Fig. $NaNbO_3$fig:phases of $NaNbO_3$hows the cubic, rhombohedral, monoclinic and orthorhombic crystal structures of $NaNbO_3$ [33]. In order to improve the use of $NaNbO_3$ in technical applications, both theoretical and experimental investigations of room temperature phases of this perovskite material is necessary.

Table 2.1: Phase transitions of $NaNbO_3$ *in various temperatures [12, 33, 34].*

Temperature [K]	Ferroelectric properties	Crystal system	Space group
T >913	PE	Cubic	$Pm\bar{3}m$
913	PE	Tetragonal	$P4/mbm$
848	PE	Orthorhombic	$Cmcm$
793	PE	Orthorhombic (S phase)	$Pnmm$
753	AFE	Orthorhombic (R phase)	$Pmnm$
633	AFE	Orthorhombic (P phase)	$Pbcm$
173	FE	Rhombohedral (N phase)	$R3c/R\bar{3}$

2.4.2 Simple Cubic $NaNbO_3$ ($Pm\bar{3}m$)

Fritsch et al. [12] obtained total energy curves for unit cell of simple cubic, rhombohedral, orthorhombic and monoclinic phases of $NaNbO_3$ by using experimental lattice parameters as initial values. Different exchange-correlation functionals have been applied. Fig. 2.5 shows total energy curves of different phases of $NaNbO_3$ with respect to equilibrium unit-cell volume obtained by applying different functionals. They calculated lattice parameter (a) and bulk moduli (B) using these energy curves for different phases of $NaNbO_3$.

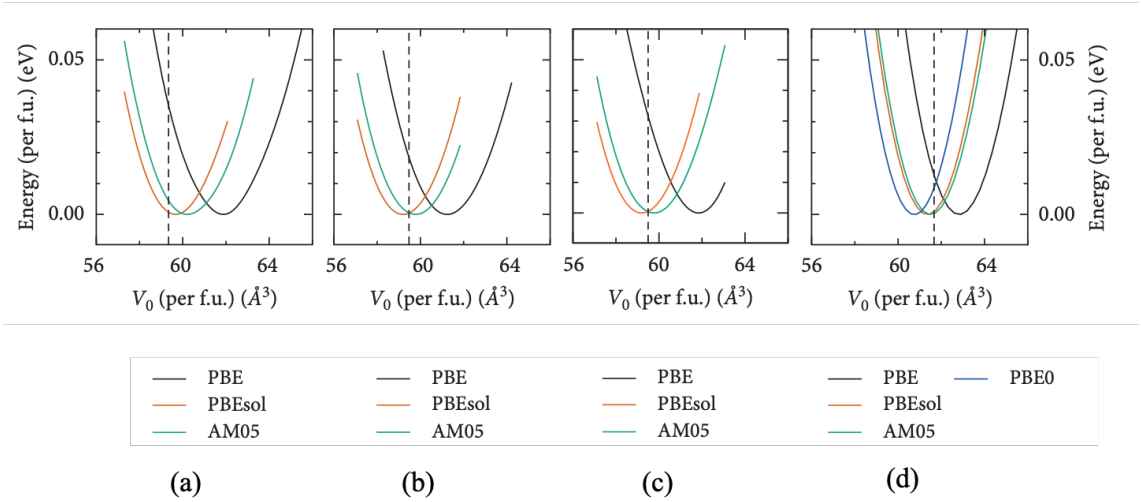

Figure 2.5: Total Energy curves for multiple crystal structures of $NaNbO_3$ *computed by using PBE, PBEsol, AM05, and PBE0 functionals; (a) rhombohedral R3c phase, (b) orthorhombic Pbcm, (c) monoclinic Pm, and (d) simple cubic* $Pm\bar{3}m$ *phase. The dashed line in the middle of each graph is experimental value of equilibrium unit-cell volume [12].*

Table 2.2 shows computed lattice parameter and bulk moduli of cubic $NaNbO_3$ using PBE, PBEsol, AM05 and hybrid functional (PBE0) in order to compare to the experimental results. Comparing the computed unit-cell volume with the available experimental results, implies that PBEsol, AM05 and PBE0 functionals yield a closer result in calculation of the lattice parameter and equilibrium unit cell volume compared to PBE functional, while they all highly overestimates the bulk moduli value. Compared to the other three functionals, PBE gives a better result regarding the value of bulk moduli when it is compared to the experimental value.

Table 2.2: Electronic and structural properties of cubic $Pm\bar{3}m$ $NaNbO_3$ *[12].*

Cubic $Pm\bar{3}m$	PBE	PBEsol	AM05	Hybrid functional (PBE0)	Experimental values
a [Å]	3.975	3.944	3.947	3.931	3.95
V [Å^3]	62.807	61.349	61.490	60.745	61.66
Band gap energy [eV] - Indirect	1.65	1.63	1.64	3.75	3.29

Fig. 2.6 shows computed band structure of cubic $NaNbO_3$ by different exchange-correlation functionals. The experimental band gap of cubic $NaNbO_3$ is measured as an indirect band gap of 3.29 eV. The calculated indirect Kohn Sham band gap of cubic $NaNbO_3$ reported by Fritsch et al. [12] (shown in table. 2.2), is 1.65, 1.63, 1.64, and 3.75 eV for PBE, PBEsol, AM05, and hybrid functional (PBE0), respectively. Comparing these values to the experimental band gap of cubic $NaNbO_3$, shows that PBE, PBEsol and AM05 functionals, highly underestimate the energy gap (up to 50%) while hybrid functional overestimate the band gap by around 15%.

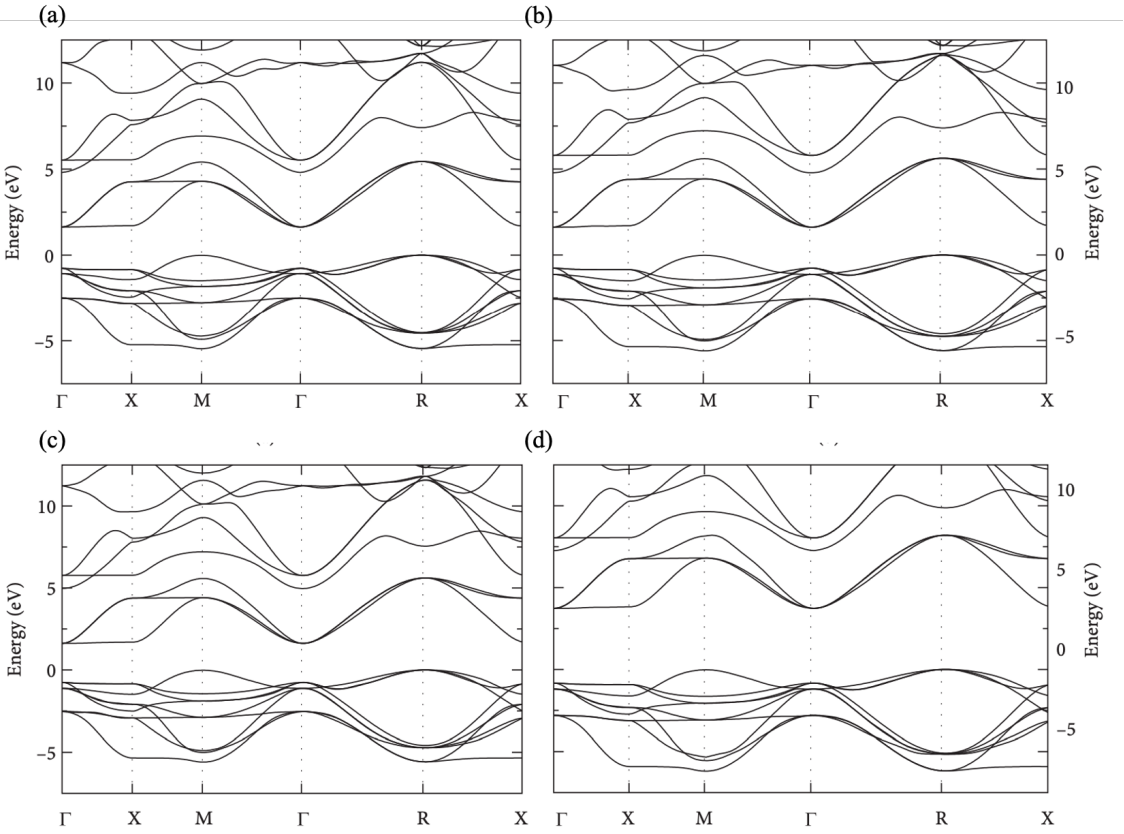

Figure 2.6: Band structures of cubic $NaNbO_3$ *computed by using different functionals; (a) PBE, (b) PBEsol, (c) AM05, and (d) hybrid functional (PBE0) [35].*

2.4.3 Rhombohedral $NaNbO_3$ ($R3c/R\bar{3}$)

Unit cell of $R3c$ phase of $NaNbO_3$ consists of 30 atoms. Fig. 2.5.a shows total energy curve of rhombohedral $R3c$ phase of $NaNbO_3$ by application of different exchange-correlation functionals. From total energy curves, lattice parameters and unit-cell volume are calculated. In Fig. 2.5.a and table $NaNbO_3$tab:Electronic and structural properties of rhombohedral $R3c$ $NaNbO_3$ it is clear that in rhombohedral phase of $NaNbO_3$ similar to cubic phase, PBE functional overestimate unit cell volume and the other two functionals (PBEsol and AM05) yields a closer result to the observed value in experimental studies [12, 36, 37]. This is worth mentioning that reported experimental values of lattice parameters in $R3c$ phase of $NaNbO_3$ by Fritsch et al. is different with what has been reported by other experimentalists [38]. Lattice parameters of $a = b = 5.33$ Å and $c = 15.62$ Å is also reported by Boukriba et al. [38] obtained from crystalline phase of rhombohedral $NaNbO_3$ using X-ray diffraction patterns.

Table 2.3: Electronic and structural properties of rhombohedral $NaNbO_3$ *(R3c) [12].*

Rhombohedral R3c	PBE	PBEsol	AM05	Experimental values
a [Å]	5.55	5.48	5.50	5.48
c [Å]	13.88	13.72	13.76	13.68
V [$Å^3$]	371.27	357.99	361.314	356.06
Band gap energy [eV] - direct	2.81	2.66	2.709	N.A.

Fig. 2.7 shows computed band structure of rhombohedral R3c phase of $NaNbO_3$ using PBEsol functional. Unfortunately, there is no experimental data available on the band gap of this phase. The calculated direct band energies of $R3c$ phase using PBE, PBEsol, and AM05 are significantly larger than the indirect band gap of cubic phase. The valence bandwidth in both cubic and rhombohedral phases are very similar.

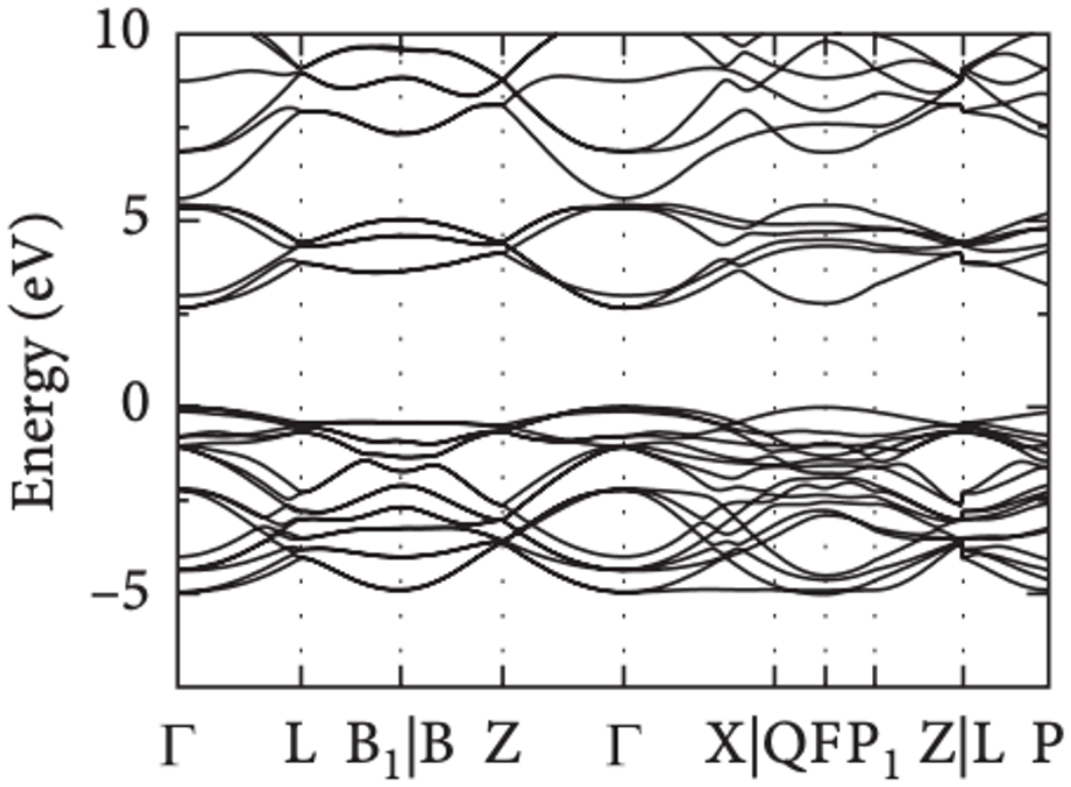

Figure 2.7: Electronic band structure of rhombohedral phase (R3c) of $NaNbO_3$*, obtained by using PBEsol functional [12].*

Chapter 3

Technical background

3.1 Density Functional Theory (DFT)

Density Functional Theory (DFT) is first suggested by Thomas and Fermi in 1927-1928 [39]. Based on their publication, this time atomic properties are completely described by electron density $n(r)$. DFT nowadays is a powerful tool in order to understand electronic and magnetic properties in solids and molecules. This method is used to approximately solve the Schrödinger equation for a many-body system. Schrödinger equation basically contains all the useful information to understand state of the system. It is solvable for simple 2D systems or Hydrogen atoms but it is not absolutely solvable for N-body systems. However, DFT makes some accurate approximations in order to solve the Schrödinger equation [40].

In DFT, instead of using wavefunction of each single electron, electron density is used (unlike HF method where the wavefunction of electron is the main function). Consider an interacting system of the electrons with an external potential of $V(r)$. Hamiltonian operator can then be written as:

$$\hat{H} = \hat{T} + \hat{U} + \hat{V} \tag{3.1}$$

Where $\hat{T}$ is the kinetic energy operator and $\hat{U}$ is Coulomb interaction operator. $\hat{V}$ is the external potential. $\hat{T}$ consists of kinetic energy of both N electrons and N nuclei. $\hat{U}$ has contribution of electron-electron interactions, nuclei-nuclei interaction and electron-nuclei interactions. Since mass of nuclei is significant compared to electron mass, based on Born-Oppenheimer (BO) approximation, we can neglect contribution of nuclei kinetic energy in $\hat{T}$ term. Consequently, nuclei position is fixed and position vector of nuclei is a constant [39–43].

3.1.1 Hohenberg-Kohn theories (HK)

In DFT, interactions between two electrons (placed in a gas of electrons) is calculated by classical Coulomb potential. Based on Hohenberg-Kohn theorems (HK theorems), any potential that is not electron-electron potential is considered as an

external potential. Ground state wavefunction (Ψ) and electron density $n(r)$ can then be calculated by substitution of Hamiltonian operator (contribution from external potentials is considered) in Schrödinger equation. Hohenberg-Kohn I and II theorems are as follow:

- **HK I theorem:** The potential of a system which is exposed to an external potential can be calculated using electron density. By having ground state density, all properties of a system can be calculated using Hamiltonian. It suggests that ground state wave function of a many body system is equal to the function of a ground state density (3.2).

$$\Psi_0(r_1, r_2, r_3, ..., r_N) = \Psi(n_0(r)) \tag{3.2}$$

  Where $n_0(r)$ is ground state electron density.

- **HK II theorem:** "A universal functional for the energy in terms of the density can be defined such that the exact ground-state energy is the global minimum of this functional and that the density that minimizes the functional is the ground-state density"(3.3) [44, 45]:

$$E[n_0] \leq E[n'] \tag{3.3}$$

  Where n' is any other density.

3.1.2 Kohn-Sham method (KS)

In a Kohn-Sham (KS) system, particles are non-interacting and they produce same density as a system with interacting particles. It is clear that finding such system will be a challenge. In KS method, we consider two systems of interacting and non-interacting particles. These two systems have the same electronic density of $n(r)$. External potential of the interacting system and non-interacting system are $V_i[n]$ and $V_{N.i}[n]$, respectively. Kinetic energy functional of an interacting system ($T_i[n]$) is sum of the kinetic energy of a non-interacting system ($T_{N.i}[n]$) plus kinetic correlation energy ($T_c[n]$), shown in equation 3.4 [46, 47].

$$T_i[n] = T_{N.i}[n] + T_c[n] \tag{3.4}$$

In order to get the total energy of an interacting system ($E_i[n]$) we need to get the sum of its kinetic energy ($T_i[n]$), Coulomb potential ($U_i[n]$) and external potential ($V_i[n]$).

$$E_i[n] = T_i[n] + U_i[n] + V_i[n] \tag{3.5}$$

Coulomb potential of an interacting system ($U_i[n]$) is contribution of exchange potential energy of electrons based on Pauli principle ($U_x[n]$), Hartree potential ($U_H[n]$) which shows Coulomb interaction of a single electron with all the N-1 electrons, and correlation potential ($U_c[n]$).

$$U_i[n] = U_x[n] + U_H[n] + U_c[n] \tag{3.6}$$

By substitution of Coulomb potential term of interacting system from 3.6 into 3.5, total energy of an interacting system will be:

$$E_i[n] = T_i[n] + U_i[n] + V_i[n] = T_{N.i}[n] + T_c[n] + U_x[n] + U_H[n] + U_c[n] + V_i[n] \quad (3.7)$$

Sum of $U_x[n]$, $U_c[n]$, and $T_c[n]$ is defined as a new term named total exchange energy ($E_x[n]$):

$$E_x[n] = T_c[n] + U_c[n] + U_x[n] \quad (3.8)$$

The total energy of an interacting system will be then turned into:

$$E_i[n] = U_H[n] + T_{N.i}[n] + E_x[n] + V_i[n] \quad (3.9)$$

In order to calculate the exchange energy, we need to use approximations. Local Density Approximation (LDA), suggests that if charge density changes slowly inside a material, we can consider that we have a homogeneous electron gas. Therefore, in the exchange energy only electronic density term is considered. However, in Generalized Gradient Approximation (GGA), along with electron density, gradient of electronic density is also considered for calculation of exchange energy. Depending on the type of material, we can use either LDA or GGA approximation. It is important to know that although GGA approximation is quite accurate in predicting the properties of molecules, it is not very precise when it comes to materials free charges such as metals or strongly correlated systems [48]. Later on, another approximation for GGA was proposed in order to calculate exchange correlation energy which includes second order gradient of electron density (PW91) [49]. PBE functional is then proposed as a more simplified GGA approximation for calculation of exchange correlation energy [50].

3.2 DFT+U method for investigation of polarons

Density Functional Theory (DFT) is a great way to predict structural properties of different materials while it fails in predicting electronic properties of semiconductors. It is impossible to calculate the precise total energy of a system using DFT as in calculation of total energy a simple approximation which is briefly discussed in section 3.1 is used for obtaining exchange correlation energy (E_x). In order to have a good approximation on total energy of the system, E_x term has to cover all the correlations and spin interactions of the system. Since it is very difficult to get to a model which E_x can precisely describe its dependence on electronic density, DFT fails in predicting the electronic properties of a system where its properties are highly controlled by many-body electronic interactions. The reason behind this error can be attributed to the fact that the applied E_x term in DFT, over-delocalize the valence electrons due to its inability to complete cancellation of electronic self-interactions. Consequently, DFT fails in predicting the properties of materials with localized charges in their system [51–53].

3.2.1 Band gap problem

The inaccuracy of DFT in predicting the electronic structure of the correlated systems is addressed as "band gap problem" [47]. The so called "Mott insulators" [54] are a group of materials which are introduced as conductive materials when their properties are measured using conventional DFT while in experimental studies they appear as insulators. This error can be due to the neglecting of electronic interactions as repulsion between electrons can localize them to the atomic orbitals and produce the observed band gap. The error is coming from the fact that the self-interaction of electrons in conventional DFT is not considered and over-delocalization of existing electrons leads to appearance of a conducting behavior. This Coulomb potential which is responsible for localization of electrons to atomic orbitals is called "U parameter". This U parameter considers the localization of charge in d and f orbitals quite well while treating the s and p orbitals by normal DFT approximations [55].

For localized electrons, charge transport occurs by a hopping mechanism where the electron jumps to its neighbor atom site. Consequently, the energy gap can be defined as [56]:

$$E_{gap} = U - 2zt \tag{3.10}$$

Where t is the hopping amplitude and z is the number of nearest neighbors. Equation 3.10 shows that as the U parameter increases, energy gap increases as well, which is sensible since higher U parameter cause high degree of electron localization to atomic orbitals. When hopping amplitude decreases, energy gap increases, consequently [56, 57].

Other models are also presented in order to describe the band structure of a correlated system. One of the simplest ones is "Hubbard model" [56], where a new term is defined in Hamiltonian to account for repulsion forces between electrons in the same atomic orbital. DFT+U method is inspired by Hubbard model in order to get a better approximation for exchange correlation functional.

In order to predict the properties of a system with localized charges LDA+U is used. Since DFT+U method treats s and p with normal DFT and Hubbard model is implemented only for d and f orbitals, the total energy of such system is summation of the total energy of the system using normal LDA plus an energy term for correlated systems (Hubbard model) [56]:

$$E_{LDA+U} = E_{LDA} + U[\rho(r)] = E_{LDA}[\rho(r)] + E_{Hub}[{n_{mm}}^{I\sigma}] - E_{dc}[n^{I\sigma}] \tag{3.11}$$

Where $E_{dc}[n^{I\sigma}]$ is the error that needs to be deducted from the total energy as energy for correlated states has been counted twice, both in normal energy term using LDA ($E_{LDA}[\rho(r)]$) and Hubbard term for correlated states ($E_{Hub}[{n_{mm}}^{I\sigma}]$).

As already mentioned above, DFT+U method is applicable on strongly correlated states in materials such as Transition Metal Oxides (TMO) where they have localized

atomic orbitals (d and f orbitals). It is worth to mention that U value needs to be kept in an optimum range as increasing U value cause over-localization of charge on the specific atomic orbital and over-flattening of band states [58]. Fig. 3.1 shows application of DFT (LDA) and DFT+U (LDA+U) for calculation of Density of States (DOS) in MnO (Fig. 3.1.a) and FeO (Fig. 3.1.b). Band energies of both MnO and FeO are underestimated using LDA, while a more precise estimation is obtained using LDA+U [59].

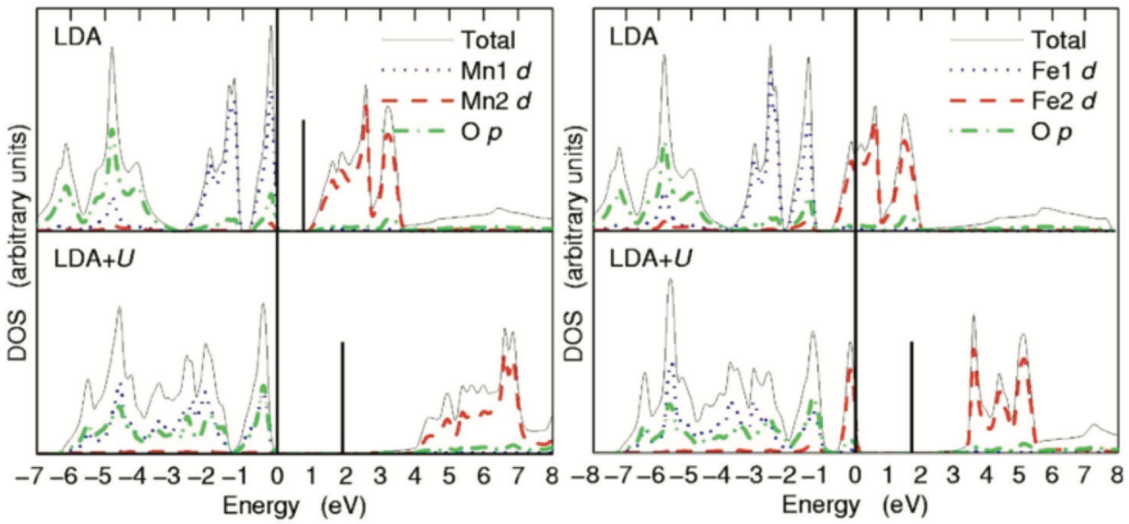

Figure 3.1: DOS plots of (a) MnO, and (b) FeO using LDA and LDA+U [59].

Different DFT parameters such as k-points mesh, cut-off energy and applied pseudopotential is very decisive in choosing the best U parameter for the desired system. Thus, calculations have to be converged with respect to both k-points mesh and cut-off energy. Presence of charge localization obtained by applying DFT+U, clearly, decrease the symmetry of system and larger k-points mesh needs to be used [58].

3.2.2 Optimization of U parameter: Piecewise linearity method

In order to use an optimum value of U parameter, computed properties can be compared to related experimental results. A theoretical alternative for optimization of U parameter for a specific system, can be piecewise linearity method where the total energy of the system is calculated with respect to the fractional charge [60].

An exact DFT method should lead to a piecewise linear response of total energy with respect to the fractional charge. However, due to the stated error in conventional DFT, there is a deviation from linear response and a convex curvature in total energy versus fractional charge patterns is observed which is due to the self-interaction error in correlated systems. In this method, total energy is obtained with respect to fractional charge of the system. Total ground-state energy of a system which consists of the fractional charge is [60]:

$$E_N = (1-\alpha)E_{N_0} + \alpha E_{N_0+1} \tag{3.12}$$

Where E_{N0} is the energy of the system with N_0 (integer) electrons, E_N is the energy of a system with fractional charge ($N = N_0+\alpha$), and α is the fractional charge.

If an exact functional was used as the exchange correlation functional instead of an approximation in DFT, a derivative discontinuity would be observed while the results obtained from normal DFT has deviation from linearity. In order to optimize U parameter, the total energy of a system with fractional charge is plotted by applying various U parameters. The U value which has a better linear response is the best choice for the studied system.

3.2.3 Hybrid functional

Most of the first principle calculations using DFT in 90s, has been done by using LDA or GGA as exchange correlation functional. These functionals give a good approximation on various electronic and structural properties of materials. Compared to the experimental data, LDA functional underestimate the lattice parameters by 1% or 2%. This may not be considered as a large error in studying different class of materials, however, for ferroelectric properties which structural properties are highly dependent on the lattice parameters (cell volume), the LDA and GGA functionals both impose some limitations on predicting the materials properties. Both LDA and GGA underestimate the electronic band structure by considering the particles independent from each other. The hybrid functionals is used to get a better prediction on bond length, atomization energy, band gaps, and excitation energies of various molecules and solids. This functional gives a better estimation on electronic properties of FE materials as well. In this section, the concept of hybrid functional is briefly discussed. As it is mentioned earlier, DFT relies on the approximation of exchange correlation functional (E_{XC}). The Hamiltonian of a system with several electron-electron interaction can be written as:

$$H_{el}(\lambda) = \hat{T} + \lambda \hat{U}_{ee} + \upsilon_\lambda \tag{3.13}$$

Where $\hat{T}_e$ is the kinetic energy operator, $\hat{U}_{ee}$ is the potential energy operator, and υ_λ is a parameter which its addition to the Hamiltonian, will cause all the Hamiltonians to produce the same ground state electron density. λ (coupling strength) is a defined parameter which shows the limit of interaction of particles. $\lambda = 0$ defines a non-interacting system while $\lambda = 1$ defines a complete interacting system. When $\lambda = 1$ and the system is fully interacting, $\upsilon_\lambda = V$, where V is the external potential. In a case where $\lambda = 0$, the $\upsilon_\lambda = V_{KS}$. V_{KS} is the Kohn-Sham potential. This way, the E_{XC} can be defined as:

$$E_{XC} = \int_0^1 E_{XC,\lambda} d\lambda \tag{3.14}$$

Where $E_{XC,\lambda}$ is defined as:

$$E_{XC,\lambda} = \left\langle \Psi_\lambda \middle| \hat{U}_{ee} \middle| \Psi_\lambda \right\rangle - E_H \tag{3.15}$$

Where Ψ_λ is the ground state wave functions, and E_H is the Hartree energy. The exhange correlation energy can be obtained from exact exchange correlation energgy ($E_{XC,\lambda=0}$) and many-body exchange correlation energy ($E_{XC,\lambda=1}$). If $E_{XC,\lambda}$ has a linear relation with

$$\lambda$$

, the exchange correlation energy could be calculated precisely as:

$$E_{XC,\lambda} = \frac{1}{2}(E_{XC,\lambda=0} + E_{XC,\lambda=1}) \tag{3.16}$$

The simple hybrid functional is then:

$$E^{hyb}_{XC,\lambda} = \frac{1}{2}(E_{XC,\lambda=0} + E^{LDA}_{XC,\lambda=1}) \tag{3.17}$$

This mixing scheme is suggested by Becke. The so called mixing scheme B3PW and B3LYP are:

$$\begin{aligned} E^{B3LYP}_{XC,\lambda} = E^{LDA}_{XC,\lambda=0} + A(E_{XC,\lambda=0} - E^{LDA}_{XC,\lambda=0}) + (1-A)B(E^{GGA}_{XC,\lambda=0} \\ -E^{LDA}_{XC,\lambda=0}) + E^{LDA}_{C} + C(E^{GGA}_{C} - E^{LDA}_{C}) \end{aligned} \tag{3.18}$$

A=0.2, B=0.8, and C=0.81 are Becke's mixing parameters for B3LYP hybrid functional and they are obtained by using experimental data. The mixing parameters for B1 hybrid functional are B=1 and C=1. Substituting these values in equation 3.18, results in:

$$E^{B1}_{XC} = E^{GGA}_{XC} + A(E_{XC,\lambda=0} - E^{GGA}_{XC,\lambda=0}) \tag{3.19}$$

Where now the equation 3.19 is more simplified with only A value as the missing parameter. The value of A is dependent on the GGA functional used in equation 3.19 [61].

Chapter 4

Technical details

DFT simulations in this thesis are done with the Vienna Ab initio Simulation Package (VASP) using projector augmented wave (PAW) pseudopotentials. Both atomic positions and cell volumes are relaxed until the maximum force acting on each atom is smaller than 0.05 $eV/\mathring{A}$ using PBE, PBEsol, and HSE06 functional. In order to visualize the atomic structures, Visualization for Electronic and Structural Analysis (VESTA) [**?**, **?**] and Open Visualization Tool (OVITO) are employed.

4.1 Rhombohedral $NaNbO_3$

4.1.1 PBE+U simulations

In the first step, atomic positions and shape of the conventional 10-atoms unit-cell of rhombohedral $NaNbO_3$ ($R\bar{3}$) is relaxed by applying U parameter of 4 eV on Nb(4d) states with energy cut off of 400 eV and k-points grid of $6 \times 6 \times 6$. In order to investigate the formation of polarons, $2 \times 2 \times 3$ supercell is then created based on the obtained relaxed structure and manually distorted. The energy of the system is then calculated in these manners by applying various U parameters:

- ${E_{pur}}_e^0$: Relaxation of atomic positions (not its volume) with a non-spin polarized calculation, energy cut off of 400 eV and k-points grid of $2 \times 2 \times 2$ on $2 \times 2 \times 3$ uniform supercell (120 atoms) of rhombohedral $NaNbO_3$ (number of electrons:720) created from relaxed 10-atoms cell in the first step..
- ${E_{dist}}^{loc(+1)}$: Relaxation of atomic positions (not its volume) with a spin polarized calculation, energy cut off of 400 eV and k-points grid of $2 \times 2 \times 2$ on $2 \times 2 \times 3$ distorted supercell (120 atoms) of rhombohedral $NaNbO_3$ (number of electrons:719) created from relaxed 10-atoms cell.
- ${E_{dist}}^{deloc(+1)}$:Relaxation of atomic positions (not its volume) with a non-spin polarized calculation, energy cut off of 400 eV and k-points grid of $2 \times 2 \times 2$ on $2 \times 2 \times 3$ supercell from former step with 719 electrons in the system.
- ${E_{pure}}^{deloc(+1)}$: Relaxation of atomic positions (not its volume) with a non-spin

polarized calculation, energy cut off of 400 eV and k-points grid of $2 \times 2 \times 2$ on $2 \times 2 \times 3$ uniform supercell (120 atoms) of rhombohedral $NaNbO_3$ (number of electrons:720) created from relaxed 10-atoms cell in the first step.

For investigation of polaron, in cases where no polaron was detected, the calculation is repeated by using relaxed system of a configuration which U(Nb4d)=4 and U(O2p)=8 is applied. This was the case for U parameters on Nb/O lower than 6 eV.

For lattice parameter comparisons, Atomic strcutre is relaxed using PBE+U starting with 10-atoms unit-cell (both atomic positions and volume are relaxed).

4.1.2 PBEsol+U simulations

In order to obtain the lattice parameters of the systems where different compositions of U parameter on Nb and O is applied, 10-atoms unit cell of rhombohedral $NaNbO_3$ is relaxed both in shape and volume with a non-spin polarized calculation, energy cut off of 400 eV and k-points grid of $6 \times 6 \times 6$.

4.1.3 Hybrid functional calculations (HSE06)

HSE06 calculations are carried out by using same energy cut off (400 eV), and k-points mesh ($2 \times 2 \times 2$) on 120-atoms supercell. Unrelaxed created pure structure at the very first step and polaronic configuration obtained by applying U(Nb4d)=4 and U(O2p)=8 using PBE+U functional are used in order to simulate a uniform structure with delocalized charge and a polaronic configuration, respectively.

4.1.4 Piecewise linearity diagrams

In order to get the total energy curves with respect to fractional charge, first the pure/distorted 120-atoms supercell is fully relaxed with removal of one electron (number of electrons:719) using PBE+U functional and resulted structure is then used for getting the energy of systems with fractional charges of 0, 0.2, 0.4, 0.6, and 0.8 eV by a single self-consistent step.

4.2 Cubic $NaNbO_3$ ($NaNbO_3$)

4.2.1 PBE+U simulations

In the first step, atomic positions and shape of the conventional 5-atoms unit-cell of cubic $NaNbO_3$ ($Pm\bar{3}m$) is relaxed by applying U parameter of 4 eV on Nb(4d) states with energy cut off of 400 eV and k-points grid of $6 \times 6 \times 6$. In order to investigate the formation of polarons, $3 \times 3 \times 3$ supercell is then created based on the obtained relaxed structure and manually distorted. The energy of the system is then calculated in the exact same way mentioned in section 4.1.1.

For investigation of polaron, in cases where no polaron was detected, the calculation is repeated by using relaxed system of a configuration which U(Nb4d)=4

and U(O2p)=8 is applied. Same as rhombohedral phase, this was the case for U parameters on Nb/O lower than 6 eV.

For lattice parameter comparisons, PBE+U calculations on 5-atoms unit-cell are carried out to fully relax the structure (both atomic positions and volume are relaxed).

4.2.2 PBEsol+U simulations

In order to obtain the lattice parameters of the systems where different compositions of U parameter on Nb and O is applied, 5-atoms unit cell of cubic $NaNbO_3$ is relaxed both in shape and volume with a non-spin polarized calculation, energy cut off of 400 eV and k-points grid of $6 \times 6 \times 6$.

4.2.3 Hybrid functional calculations (HSE06)

HSE06 calculations are carried out by using the same energy cut off (400 eV) in the entire simulation, and k-points mesh ($3 \times 3 \times 3$) on 135-atoms supercell. Unrelaxed created pure structure at the very first step and polaronic configuration obtained by applying U(Nb4d)=4 and U(O2p)=8 using PBE+U functional are used in order to simulate a uniform structure with delocalized charge and a polaronic configuration, respectively.

4.2.4 Piecewise linearity diagrams

Similar to the method applied on $R\bar{3}$, in order to get the total energy curves with respect to fractional charge, first the pure/distorted 120-atoms supercell is fully relaxed with removal of one electron (number of electrons:719) using PBE+U functional and resulted structure is then used for getting the energy of systems with fractional charges of 0, 0.2, 0.4, 0.6, and 0.8 eV by a single self-consistent step.

Chapter 5

Results and Discussion

$NaNbO_3$ is investigated in its two phases of rhombohedral ($R\bar{3}$) and simple cubic ($Pm\bar{3}m$) in order to shed light on the existence of self-trapped hole-polarons (STH) by using DFT+U and hybrid functional (HSE06).

5.1 Rhombohedral $NaNbO_3$

5.1.1 Pure structure

In order to avoid any misconception, the relaxed lattice structure of $NaNbO_3$ obtained by relaxing the supercell of $NaNbO_3$ with no charge or distortion in the system, is referred to as pure structure/ideal structure in this Master thesis. The structure which hole-polaron appears as a result of an applied distortion and removal of one electron from the lattice, is addressed as polaronic configuration. Similarly, other configurations can be easily defined based on these two configurations.

Fig. 5.1 shows band structure and density of states in the pure structure of rhombohedral $NaNbO_3$ using PBE+U and PBEsol+U functionals. Fig. 5.1.a and b show band structure (BS) and density of states (DOS) of $R\bar{3}$ $NaNbO_3$ using PBE+U functional with U parameter of 4 eV on Nb(4d) states. The obtained band gap using PBE+U and PBEsol+U functionals are indirect band gap of 4.49 eV and 4.21 eV, respectively. Due to the application of PBE+U functional the band gap energy is not highly underestimated in contrast with the use of conventional PBE. Unfortunately, there is no data available on experimental results regarding band energy of rhombohedral $NaNbO_3$. The computed band gap of $R\bar{3}$ phase using HSE06 calculations is 5.15 eV.

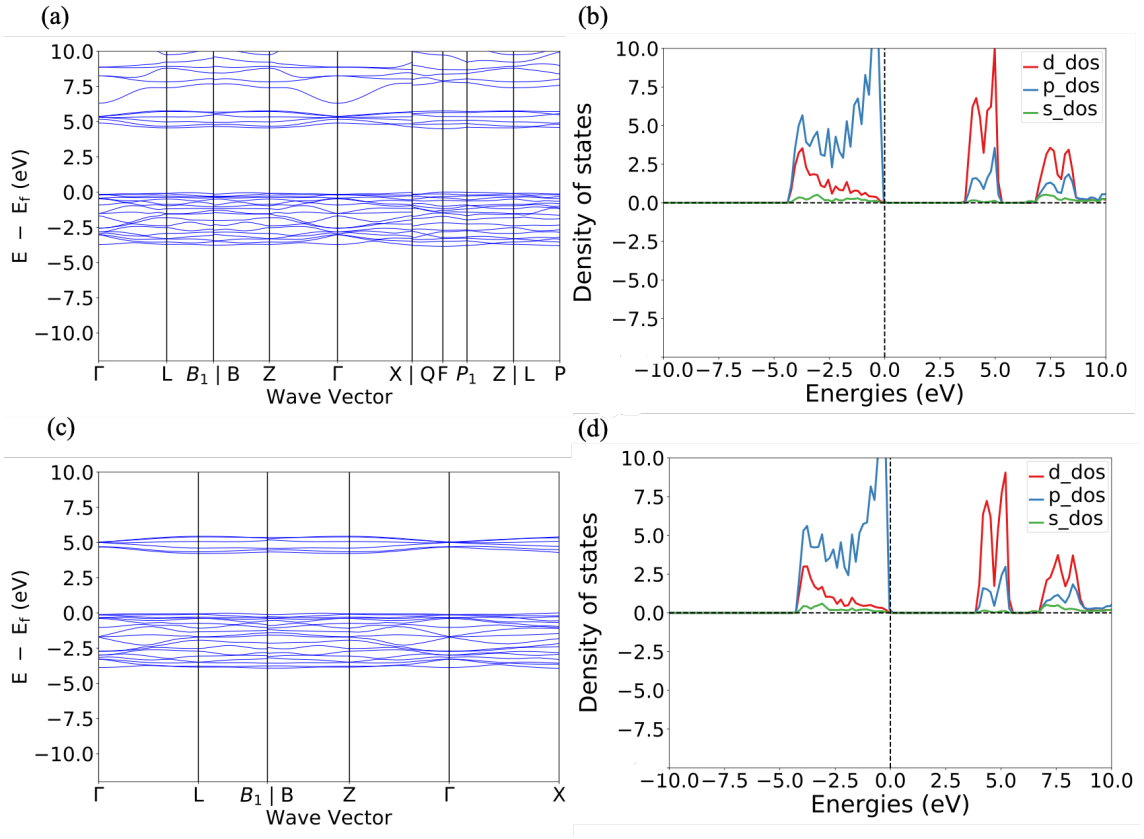

Figure 5.1: Electronic properties of pure structure of rhombohedral $NaNbO_3$ *obtained using (a, b) PBE functional, and (c, d) PBEsol functional.*

5.1.2 Polaron appearance

For studying the formation of polaron in rhombohedral $NaNbO_3$, $2 \times 2 \times 3$ supercell (120 atoms) is employed. Initial relaxation is done on pure lattice structure of $NaNbO_3$ using PBE+U by applying U parameter of 4 eV on Nb(4d) states. At the next step, in order to get a self-trapped hole polaron (STH), relaxed lattice is manually distorted. Three oxygen atoms are randomly displaced toward Nb atom in the center by 0.15 Å (7.5 %) . Fig. 5.2 shows how lattice is manually distorted compared to the pure relaxed structure. One electron is then removed from the lattice. The structure is re-relaxed using PBE+U functional with U parameters of 4 eV on Nb(4d) states and 2, 4, 6, 8, 10, and 12 eV on O(2p) states.

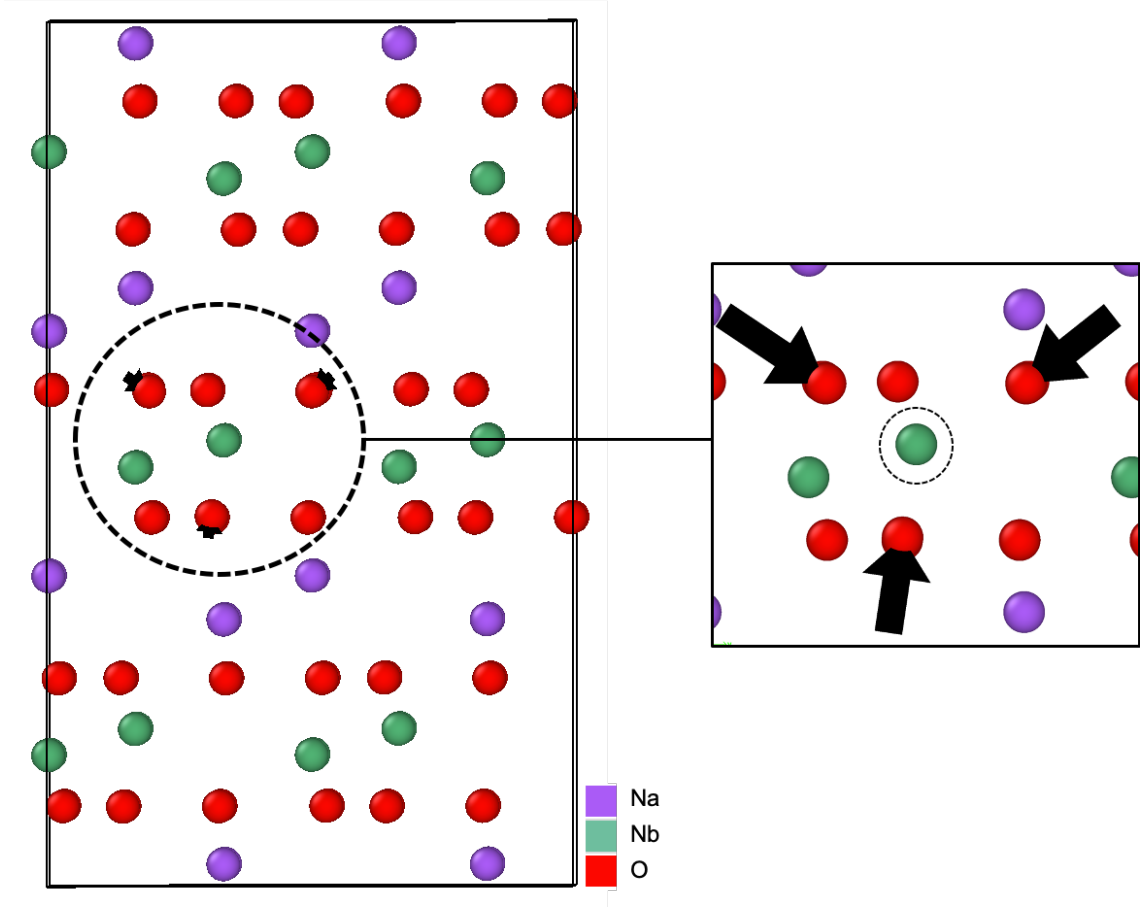

Figure 5.2: Applied manual distortion on relaxed pure structure of rhombohedral $NaNbO_3$ *in 2×2×3 supercell. Oxygen atoms are displaced by 0.15 Å (7.5 %) inward toward Nb atom in the center.*

Acquired results from PBE+U calculations show the localization of charge on 2p orbital of an O atom around target Nb (atom number 46) for cases where U parameter of 4 eV is applied on Nb atoms and where U parameter on O is larger than 2 eV.

Fig. 5.3 shows the final displacements of atoms in 2×2×3 supercell of rhombohedral $NaNbO_3$ after full relaxation of the system and table 5.1 shows the magnetisation of O atoms in the polaronic site and their relative displacement compared to the ideal supercell. Due to concentration of positive charge on O atom (number 101) which has magnetization of 0.766, some O atoms has moved toward this large positive charge (O number 114 and 117) and cations have moved away. Displacement of atoms toward and further away from the O atom 101 is indicated with + and - sign in the table 5.1, respectively.

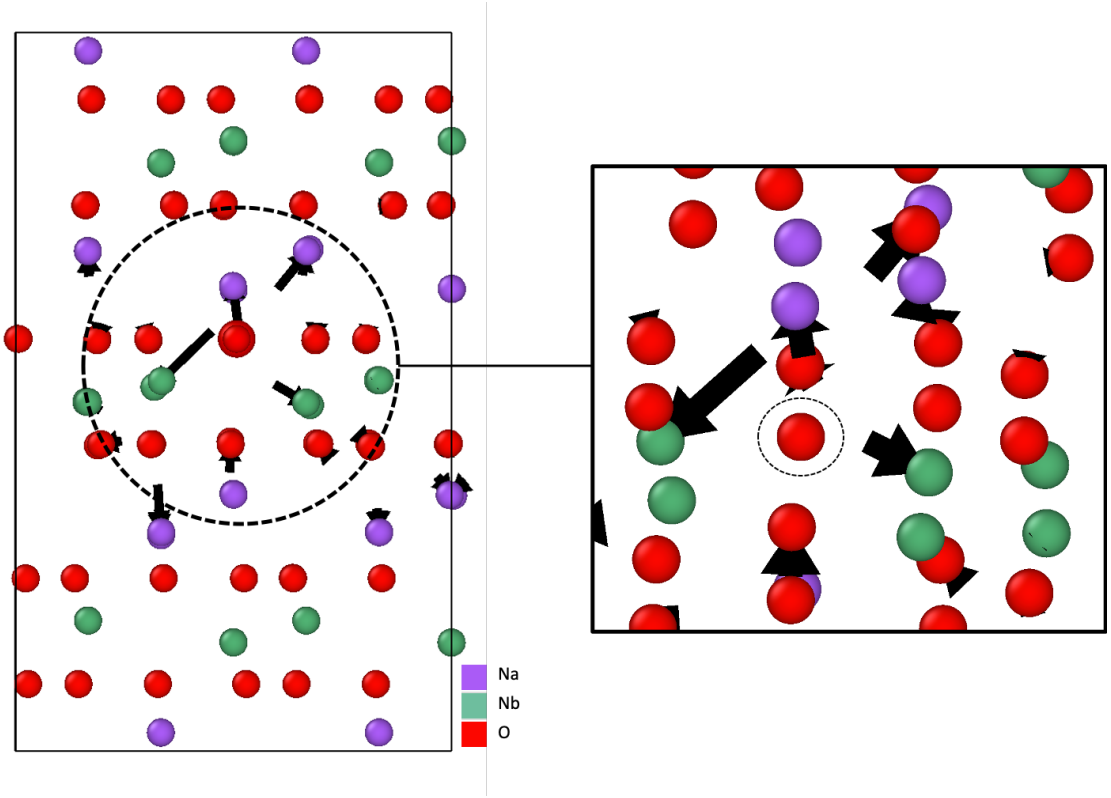

Figure 5.3: Schematic illustration of displacement of atoms after relaxation of ideal supercell with one excess positive charge in the rhombohedral system; O atoms around the O in the center are slightly displaced. The O atom which polaron is formed on, is circumvented by a dashed line.

Table 5.1: Displacements and magnetization of Nb, Na and O atoms in the polaronic site in 2×2×3 supercell of rhombohedral $NaNbO_3$.

Atom type	Number	Displacement [Å]	Magnetisation
Nb	46	-0.198683	0
Na	23	-0.132857	0
O	101	0.0153877	0.766
O	114	+0.0783173	0.03
O	117	+0.0567183	0.03

Fig. 5.4 shows partial charge density on different atoms in pure and polaronic configurations. The localization of hole mostly on a single O atom is obvious in Fig. 5.4.b, unlike equal distribution of positive charge density on all the O atoms in the pure structure of $NaNbO_3$ (Fig. 5.4.a). Positive charge is highly localized on one O atom in polaronic configuration. This charge localization is formed due to the strong coupling of charge to the lattice (Fig. 5.4.b). This leads to smaller charge density on neighbouring O atoms. O atoms around the one which contains the highest localization of charge, has higher magnetisation compared to the rest of the O atoms in the system (5.1).

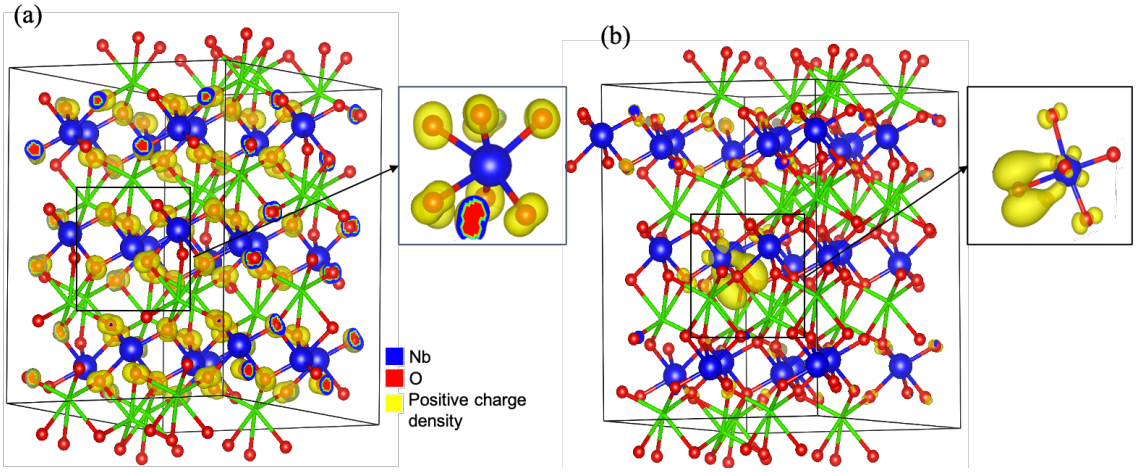

Figure 5.4: Schematic illustration of partial charge density in (a) pure structure, and (b) polaronic configuration of rhombohedral $NaNbO_3$.

Fig. 5.5 shows PDOS plots and BSs in 2×2×3 supercell of distorted rhombohedral $NaNbO_3$, obtained by applying U parameter of 4 eV on Nb(4d) states and various U parameters of 2, 4, 6, 8, 10, and 12 eV on O(2p) states. Applied manual distortion shown in Fig. 5.2 along with one positive charge (hole) in the lattice has led to the appearance of a localized level, shown in Fig. 5.4, which is located on 2p orbital of one oxygen atom. As indicated in Fig. 5.5a and b, U=2 eV on O(2p) states does not lead to formation of polaronic level in 2×2×3 supercell of rhombohedral $NaNbO_3$ as this U value is too small to maintain the charge in a localized state. In-gap STH level is clearly observed for U parameters larger than 2 eV on O. Table 5.2 shows that how position of the STH level is changing with respect to the VBM by increasing the U parameter on O(2p) states. As mentioned in section 3.2, DFT tends to over-delocalize the valence electrons/holes in the lattice. Applying U parameter on atomic orbitals leads to compensation for self-interaction error caused by the use of DFT and encourages the system to localize the charges. By increasing U parameter on 2p states of O atoms, the system tends to localize the charge relative to applied value of U parameter which accounts for acquired results shown in table 5.2. In high values of U (O2p) namely 8, 10, and 12 eV, the in-gap STH level is closer to the CBM which is due to higher localization of STH. It is worth mentioning that both too high and too low values of U, leads to unrealistic data in the final results. Inspecting magnetization of each system with different U parameter according to the table 5.2, shows that the additional positive charge is distributed over the whole lattice for a case where U parameter is small and charge is still over-delocalized. As a result, no polaron is formed, while for higher values of U, charge density is mostly concentrated on a single oxygen in the distorted area and remaining charge is delocalized through other O atoms.

Table 5.2: Total magnetization, STH level with respect to VBM for polaronic configurations of 2×2×3 supercell in rhomboheral $NaNbO_3$ *with U(Nb4d)=4 eV and various U(O2p).*

U (O2p) [eV]	U(Nb4d) [eV]	STH level with respect to VBM	Total Magnetisation	Magnetisation on O (atom 101)
4	2	-	0.840	0.017
4	4	0.57	0.809	0.695
4	6	1.25	0.808	0.742
4	8	1.83	0.812	0.766
4	10	2.32	0.817	0.783
4	12	2.71	0.824	0.798

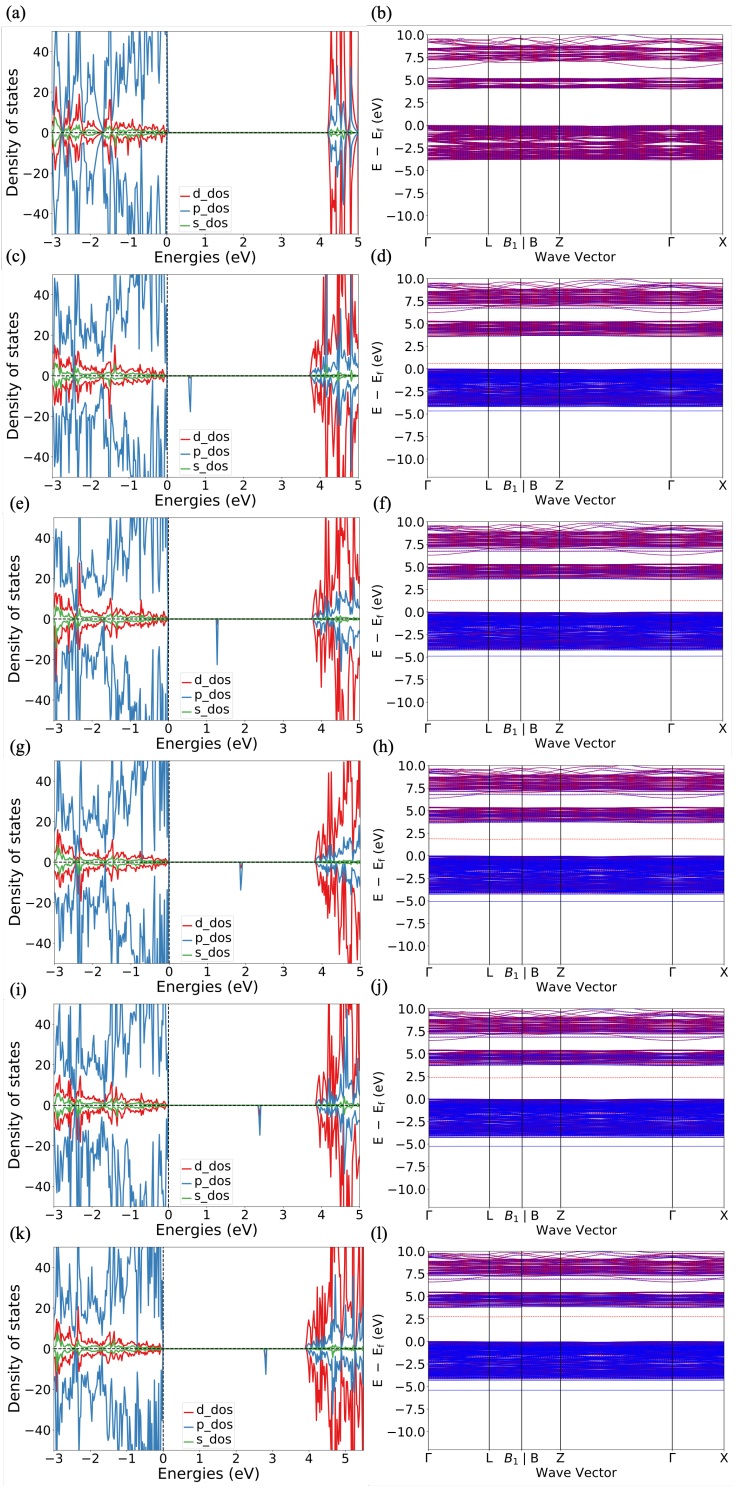

Figure 5.5: Partial density of states (PDOS) and band structure (BS) obtained by applying U parameter of 4 eV on Nb(4d) states and different U parameters on O(2p) states in 2×2×3 supercell in rhomboheral $NaNbO_3$*; (a) PDOS for U=2 eV on O(2p) states, (b) BS for U=2 eV on O(2p) states, (c) PDOS for U=4 eV on O(2p) states, (d) BS for U=4 eV on O(2p) states, (e) PDOS for U=6 eV on O(2p) states, (f) BS for U=6 eV on O(2p) states, (g) PDOS for U=8 eV on O(2p) states, (h) BS for U=8 eV on O(2p) states, (i) PDOS for U=10 eV on O(2p) states, (j) BS for U=10 eV on O(2p) states, (k) PDOS for U=12 eV on O(2p) states, (l) BS for U=12 eV on O(2p) states.*

5.1.3 Polaron energy regimes and configuration coordinate diagram

In order to investigate the stability of the aforementioned polaron, studying energetics and structural distortions of the lattice is necessary. To better understand various definitions discussed in the literature, we first further discuss how to characterize a polaronic system. In the polaronic system, the excess charge carrier appears to be an integer which is localized on one atom (specific orbital), that is why DFt+U or hybrid functional calculations need to be done in a spin-polarized manner. On the other hand, when the excess charge is delocalized, the charge density is distributed through the whole lattice and is in the form of a fractional charge [62, 63].

A polaron is energetically stable in the system when the energy of the system associating with a localized charge and structural distortion is lower compared to the system where the charge is delocalized over the whole lattice. Total energy of the system associated with existence of a localized or a delocalized charge carrier can be computed using different energy regimes. Since there are many misnomers for the definition of different configurations, each configuration is defined with details in this section [63]:

- $\mathrm{E}^{0}_{\mathrm{pure}}$: Total energy of a system where lattice is uniform and there is no excess charge in the system.
- $\mathrm{E}^{\mathrm{loc}}_{\mathrm{dist}}$: Total energy of a system where lattice is distorted and excess charge is localized to a single site. In this study such configuration is referred to as polaronic configuration.
- $\mathrm{E}^{\mathrm{deloc}}_{\mathrm{dist}}$:Total energy of a system where lattice is distorted and excess charge carrier is delocalized.
- $\mathrm{E}^{\mathrm{deloc}}_{\mathrm{pure}}$: Total energy of a system where lattice is uniform and the excess charge carrier is delocalized.

This needs to be taken into account that in order to have a localized charge in the system, computations have to be done in a spin polarized manner while delocalized charge in a distorted system can be achieved by a non-spin polarized calculation.

Considering definitions above, trapping energy of a polaron (E_{trap}), strain energy (E_{ε}), and electronic energy (E_{el}) are defined as follow [63]:

- E_{Trap}: Trapping energy of a polaron is defined as the energy difference of the distorted system with a localized charge (${E_{dist}}^{loc(+1)}$) and uniform lattice with delocalized charge (${E_{pure}}^{deloc(+1)}$). The polaron is energetically stable if the total energy of the polaronic configuration (${E_{dist}}^{loc(+1)}$) is more negative compared to the ${E_{pure}}^{deloc(+1)}$. This means that the system prefers to be in the state where charge is localized on one site rather than being distributed over the entire structure.

$$E_{trap} = {E_{dist}}^{loc(+1)} - {E_{pure}}^{deloc(+1)} \tag{5.1}$$

- E_{ε}: Strain energy is attributed to the amount of energy needed to distort the lattice in a way that it can trap the excess charge carrier.

$$E_{\varepsilon} = {E_{dist}}^{deloc(+1)} - {E_{pure}}^{deloc(+1)} \tag{5.2}$$

- E_{el}: Electronic energy is the gained amount of energy due to localization of charge.

$$E_{el} = {E_{dist}}^{loc(+1)} - {E_{dist}}^{deloc(+1)} \tag{5.3}$$

Normally, the STH formation energy can be calculated using E_{Trap}, by the energy difference of the configuration with distorted lattice plus a localized charge (${E_{dist}}^{loc(+1)}$) and a neutral system (ideal supercell) with a delocalized charge (${E_{pure}}^{deloc(+1)}$). These configurations have both same number of electrons in their system. Since there is a half-filled state in computation of energy for ${E_{pure}}^{deloc(+1)}$, the value we obtain from equation 5.1 is dependent on k-point grids of the calculation. Alternatively, by considering the polaron as a defect in the supercell, we can calculate the formation energy of STH using defect thermodynamics by equation 5.4 [6]:

$$E_{form} = {E_{dist}}^{loc(+1)} - {E_{pure}}^{0} + qE_{VBM} \tag{5.4}$$

Where E_{form} is the formation energy of the STH, ${E_{pure}}^{0}$ is the energy of ideal supercell with no excess charge, q is the excess charge (which in this study is equal to +1) and E_{VBM} is the VBM in the ideal supercell. In this case since all the states are either fully-empty or fully-occupied, the dependence on k-point grid will vanish. Since in this study, the formation energy of STH is not converged with respect to number of k-points grid, for having a better approximation on formation energy of STH, it is calculated using both equations 5.1 and 5.4.

Table 5.3 shows different energy regimes of 2×2×3 supercell in rhombohedral $NaNbO_3$. Trapping energy can be obtained by sum of the electronic energy and strain energy. By increasing U parameter and localization of charge density to a specific atom, the energy gained due to the localization of charge increases and the charge will be more bound to the formed potential well. Consequently, trapping energy of polaron will increase by increasing relative U parameter.

Trapping energy for the configuration where U parameter on both Nb(4d) states and O(2p) states is 4 eV, is very small amount of 0.04 eV which implies that the appeared polaron might be a metastable configuration. For higher U parameters on O(2p) states, trapping energy significantly increases and makes the polaronic configuration stable compared to the pure structure with a delocalized charge. Since trapping energy and formation energy calculated by using thermodynamics of defects (5.4) are very close to each other, it can be deduced that the error for using equation 5.1 is very small and expensive computations of increasing k-points grid of the system is not necessary.

Configuration coordinate diagram of a stable STH is shown in Fig. 5.6 where U parameter of 4 eV on Nb(4d) states and 6 eV on O(2p) states is applied.

Table 5.3: Polaron energy regimes for various U parameters in 2×2×3 supercell of rhomboheral $NaNbO_3$.

U (Nb4d) [eV]	4	4	4	4	4
U (O2p) [eV]	4	6	8	10	12
Trapping Energy [eV]	-0.08	-0.38	-0.74	-1.11	-1.50
Strain Energy [eV]	0.00	+0.03	+0.04	+0.04	+0.05
Electronic energy [eV]	-0.08	-0.41	-0.78	-1.15	-1.55
Formation Energy based on Eq. 5.4 [eV]	-0.07	-0.41	-0.78	-1.16	-1.56

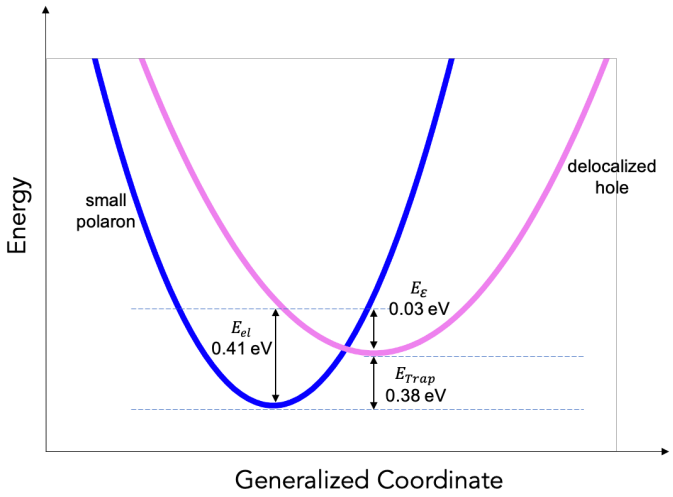

Figure 5.6: Configuration coordinate diagram for formation of stable small polaron in 2×2×3 distorted supercell of rhomboheral $NaNbO_3$ *by applying U parameter of 4 eV on Nb(4d) states and U parameter of 6 eV on O(2p) states.*

5.1.4 Piecewise linearity diagrams

Fig. 5.7 shows piecewise linearity behavior of 2×2×3 supercell of rhombohedral $NaNbO_3$ with the use of polaronic configuration as the initial structure. U parameter on Nb(4d) is kept constant to the values of 2, 4, 6, 8, 10 and 12 eV while U parameter on O(2p) states is changing. The optimum value of U parameter applied on a system with an initial distortion (Fig. 5.7.a) is U(Nb4d) = 2 eV and U(O2p) = 2, 6, and 8 eV. For U parameter of 4 eV on Nb(4d) states, optimum value of U parameter on O(2p) states are 2, 6, and 8 eV, respectively (shown in the Fig. 5.7.b). For U parameter of 6 eV on Nb(4d) states, optimum value of the U parameter on O(2p) states are similarly 2, 6, and 8 eV, respectively (Fig. 5.7.c). U parameter of 8 eV on Nb(4d) states, yields the same result as U(Nb4d)=4 eV and U(Nb4d)=6 eV. The best U on O(2p) states for U(Nb4d) equal to 10 and 12 eV, are 2, 4, and 6 eV, respectively. U parameters larger than 6 eV on O(2p) is too large and may results in overlocalization of charge. All the proper U parameters applied on Nb and O atoms are compared in Fig. 5.8. Since several composition of U parameters on Nb and O are in agreement with the criteria of piecewise linearity method:

- U(Nb4d)=4 eV, U(O2p)=4 eV

- U(Nb4d)=4 eV, U(O2p)=2 eV
- U(Nb4d)=6 eV, U(O2p)=4 eV
- U(Nb4d)=6 eV, U(O2p)=2 eV

lattice parameters and energy band gap of each system need to be compared to the available experimental values. Table 5.4 shows the existence of polaron, computed lattice parameters by using PBE and PBEsol functional and band gap energy (by PBE) for different compositions of U parameter on Nb and O. Considering the experimental lattice parameters of rhombohedral $NaNbO_3$ as $a = 5.332\mathring{A}$ and $c = 15.62\mathring{A}$ ([38]), since the STH polaron does not exist when U parameter of 2 eV is applied on O, the best options for choice of U parameter is:

- U(Nb4d)=4 eV, U(O2p)=4 eV
- U(Nb4d)=6 eV, U(O2p)=4 eV

Both options above, yield the band gap energy which are in a good agreement with the data proposed by Fritsch et al.

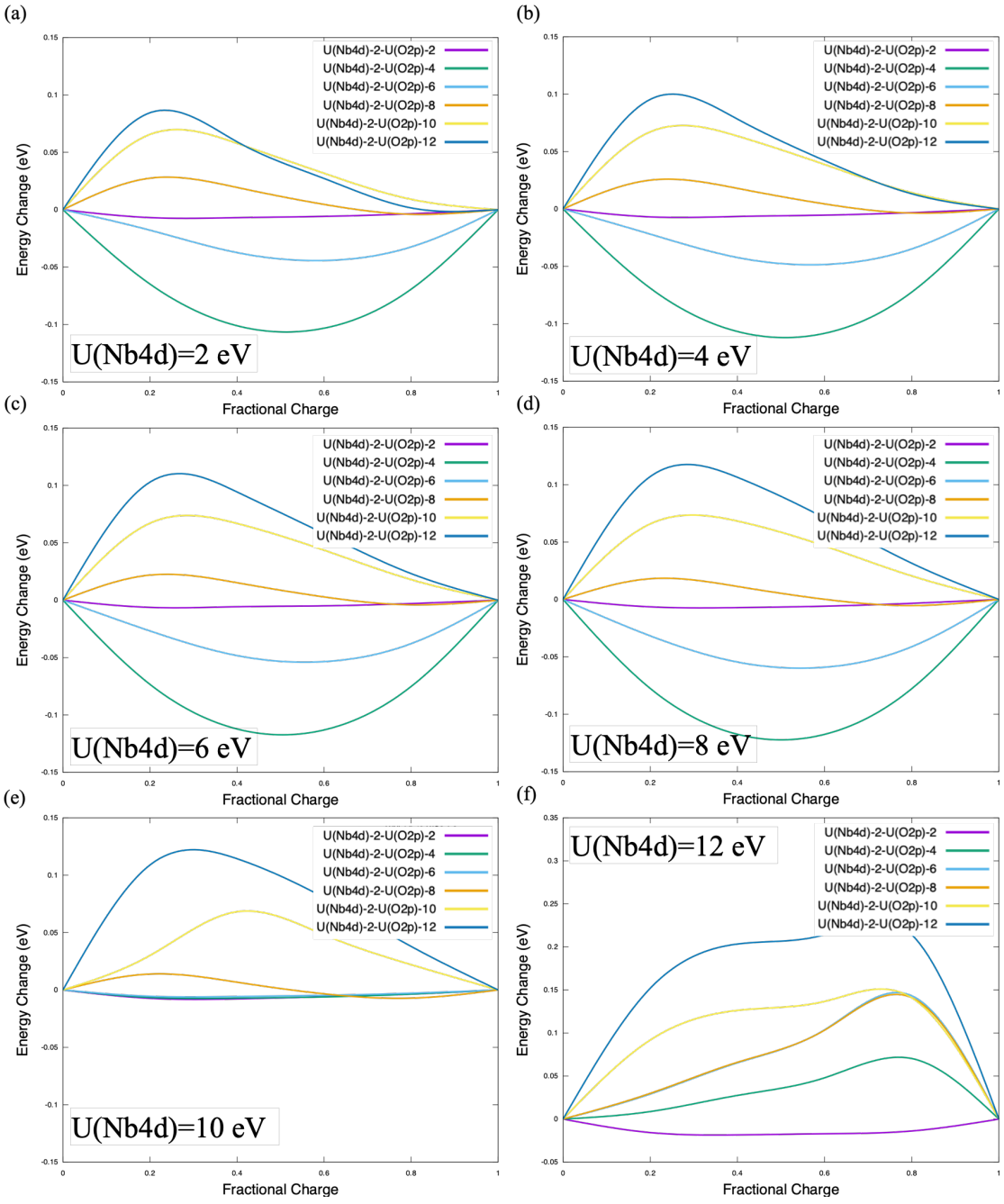

Figure 5.7: Application of various U parameters on Nb(4d) and O(2p) states, simultaneously on polaronic configuration of 2×2×3 supercell of rhombohedral $NaNbO_3$.

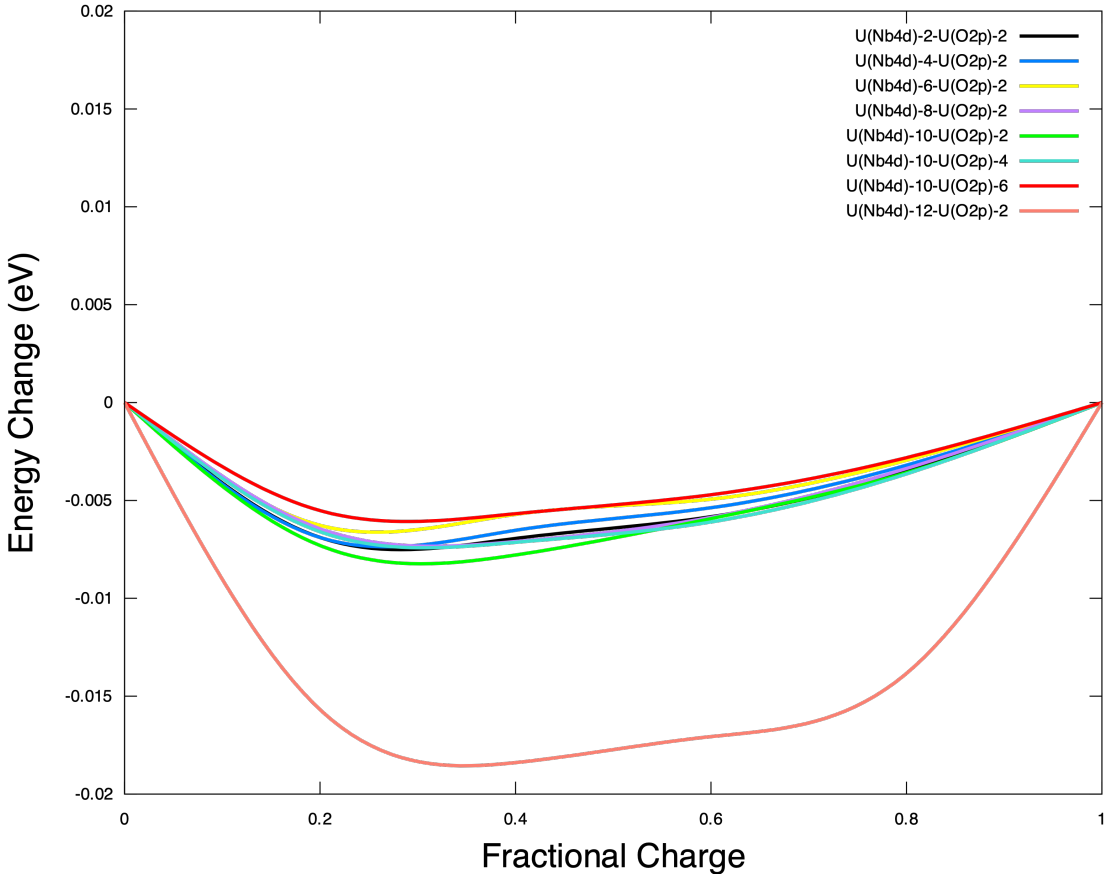

Figure 5.8: Comparison of piecewise linearity behavior of the total energy with respect to the fractional charge of 2×2×3 supercell in rhombohedral $NaNbO_3$ *by applying different U parameters on both Nb(4d) and O(2p) states using the polaronic configuration as the initial system.*

Table 5.4: Investigation of existence of polaron in different compositions of U parameters on Nb and O, lattice parameters and energy band gap obtained using PBE and PBEsol in 2×2×3 supercell of rhombohedral $NaNbO_3$.

			Lattice Parameters [Å] (PBE-supercell)		Lattice Parameters [Å] (PBEsol-conventional cell)		Lattice Parameters [Å] (PBEsol-unitcell)		
U(Nb4d) [eV]	U(O2p) [eV]	Existence of Polaron	a	c	a	c	a	c	Band Gap [eV]
2	2	No	10.74	15.40	5.31	14.99	5.31	15.06	3.9545
2	4	Yes	10.82	15.89	5.41	15.89	5.34	15.24	3.9665
2	6	Yes	10.70	15.23	5.30	14.96	5.30	14.94	4.0557
2	8	Yes	10.68	15.24	5.30	14.95	5.28	14.94	4.1083
2	10	Yes	10.68	15.21	5.29	14.94	5.29	14.91	4.1625
2	12	Yes	10.66	15.20	5.29	14.92	5.28	14.91	4.2213
4	2	No	10.76	15.33	5.38	15.27	5.36	15.18	4.0168
4	4	Yes	10.74	15.28	5.38	15.43	5.36	15.18	4.0667
4	6	Yes	10.74	15.31	5.37	15.26	5.35	15.18	4.1147
4	8	Yes	10.78	15.26	5.37	15.23	5.36	15.18	4.1575
4	10	Yes	10.72	15.24	5.36	15.23	5.36	15.18	4.2146
4	12	Yes	10.70	15.27	5.35	15.20	5.34	15.15	4.2835
6	2	No	10.80	15.33	5.36	15.00	5.36	15.03	4.1071
6	4	Yes	10.80	15.35	5.36	15.00	5.35	15.03	4.1621
6	6	Yes	10.78	15.30	5.35	15.01	5.35	15.03	4.2025
6	8	Yes	10.78	15.32	5.35	15.00	5.34	15.00	4.2655
6	10	Yes	10.76	15.30	5.34	15.00	5.34	15.00	4.3239
6	12	Yes	10.76	15.29	5.33	14.99	5.33	14.97	4.3787
8	2	No	10.86	15.36	5.38	15.05	5.38	5.02	4.1948
8	4	Yes	10.84	15.35	5.38	15.04	5.37	15.03	4.2519
8	6	Yes	10.84	15.33	5.38	15.04	5.37	15.03	4.2988
8	8	Yes	10.82	15.33	5.37	15.04	5.36	15.03	4.3686
8	10	Yes	10.82	15.33	5.36	14.97	5.36	15.03	4.4327
8	12	Yes	10.80	15.30	5.36	15.00	5.35	15.00	4.492
10	2	No	10.90	15.38	5.41	15.08	5.40	15.06	4.3134
10	4	No	10.90	15.37	5.41	15.07	5.39	15.06	4.3677
10	6	Yes	10.88	15.35	5.40	15.05	5.39	15.06	4.4268
10	8	Yes	10.88	15.36	5.39	15.04	5.38	15.06	4.4968
10	10	Yes	10.86	15.35	5.39	15.03	5.38	15.06	4.563
10	12	Yes	10.86	15.32	5.38	15.07	5.37	15.06	4.6361
12	2	No	10.94	15.44	5.43	15.13	5.42	15.06	4.4818
12	4	No	10.92	15.43	5.43	15.09	5.41	15.06	4.5405
12	6	Yes	10.94	15.38	5.42	15.08	5.40	15.06	4.5863
12	8	Yes	10.92	15.36	5.42	15.05	5.40	15.06	4.6533
12	10	Yes	10.92	15.35	5.41	15.04	5.40	15.06	4.7219
12	12	Yes	10.90	15.34	5.41	15.03	5.39	15.03	4.8909

5.1.5 HSE06 calculations

The formation of the polaron is also investigated using HSE06 functional. The polaronic configuration of PBE+U with U parameter of 4 eV on Nb(4d) states and U parameter of 8 eV on O(2p) states is used as the initial configuration in order to do a hybrid functional calculation. Fig. 5.9 shows the density of states plots of the polaronic configuration of rhombohedral $NaNbO_3$ and its pure structure with a delocalized charge. The polaronic state is clearly observable at the energy level of 2.01 with respect to VBM. the magnetisation on O(2p) is 0.733 which is in a very good agreement with PBE+U functional with application of U(Nb4d)=4 and U(O2p)=8 eV. The trapping energy of polaron is calculated by using the equation 5.1 and comparison of the total energy of the polaronic configuration and the ideal cell with a delocalized charge. The E_{trap} of STH with application of HSE06 functional is +0.25 eV. The positive trapping energy implies that polaronic state in this phase is a metastable phase which is not in consistent with the data obtained by PBE+U functional. This inconsistency can be due to the use of PBE+U configuration for the initial atomic positions of HSE06 calculations. The relaxation procedure is once tested by HSE06 along with the applying a manual distortion (5.1.2) to the system, however, the applied distortion which leaded to the formation of polaron in PBE+U functional, did not result in formation of STH polaron with the use of HSE06. The formation energy of polaron calculated by using equation 5.4 is -0.62 eV. as mentioned earlier, the formation energy of STH polaron obtained by using PBE+U with U(Nb4d)=4 and U(O2p)=8 eV, is -0.78 eV. The data obtained from these two functionals are in reasonable agreement, considering that HSE06 calculations takes 2-3 orders of magnitude more computing time. Regarding the

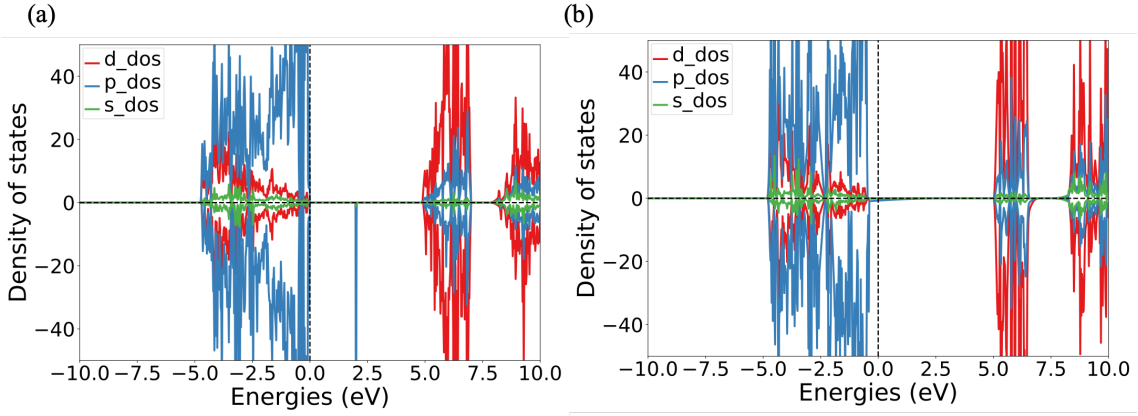

Figure 5.9: PDOS plots of rhombohedral $NaNbO_3$ *obtained by using HSE06 functional; (a) PDOS plot of the STH configuration, and (b) PDOS plot of ideal supercell with a delocalized hole.*

5.2 Cubic $NaNbO_3$

The existence of polaron using DFT+U is also investigated in cubic phase of $NaNbO_3$ ($Pm\bar{3}m$). Cubic phase of $NaNbO_3$ has paraelectric properties as mentioned in the

section 2.4.1. the formation of polaron is investigated using PBE+U and HSE06 functionals. However, the applied manual distortion did not lead to appearance of any polaron in the supercell of cubic $NaNbO_3$. Other types of distortions can be investigated in the future studies.

5.2.1 Pure structure

Fig. 5.10 shows band structure and density of states in the pure structure of cubic $NaNbO_3$ using PBE+U and PBEsol+U functionals. Fig. 5.10.a and b show band structure (BS) and density of states (DOS) of $Pm\bar{3}m$ $NaNbO_3$ using PBE+U functional with U parameter of 4 eV on Nb(4d) states. The obtained band gap using PBE+U and PBEsol+U functionals are indirect band gap of 1.39 eV and 2.09 eV, respectively. These values are in agreement with the data reported by Fritsch et al. the experimental band gap energy of $Pm\bar{3}m$ is 3.29 eV and as expected both PBE+U and PBEsol+U highly underestimated the band gap energy. eV [12, 38].

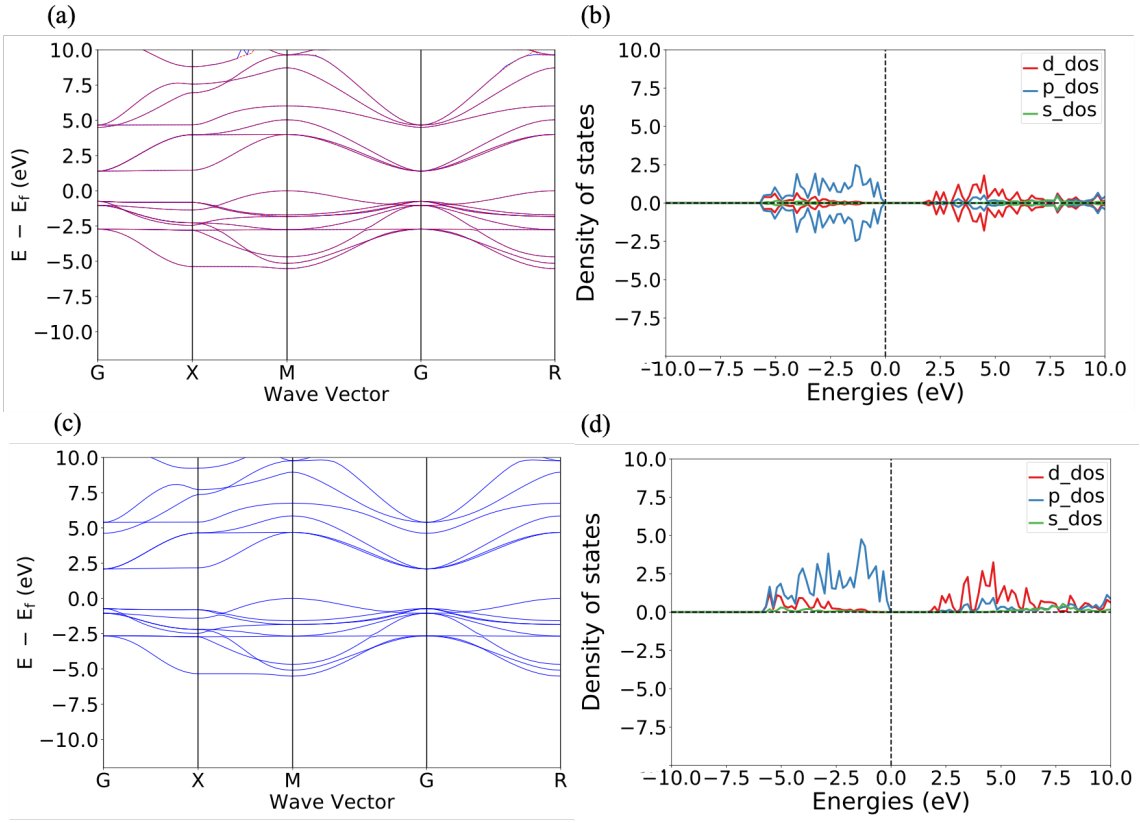

Figure 5.10: Electronic properties of pure structure of cubic $NaNbO_3$ *obtained using(a, b) PBE functional, and (c, d) PBEsol functional.*

5.2.2 Polaron appearance

Same method as rhombohedral $NaNbO_3$ is used for investigation of existence of polaron in the cubic phase. The unit cell of cubic $NaNbO_3$ is relaxed both in atomic positions and shape with PBE+U functional with U parameter of 4 eV on Nb(4d)

states. The relaxed structure is then used to create a 3×3×3 supercell with 135 atoms. Fig. 5.11 shows how the created supercell is manually distorted by moving O atoms toward an O atom in the center (the one circumvented by dashed line) and cations (Nb and Na) are moved further away from it.

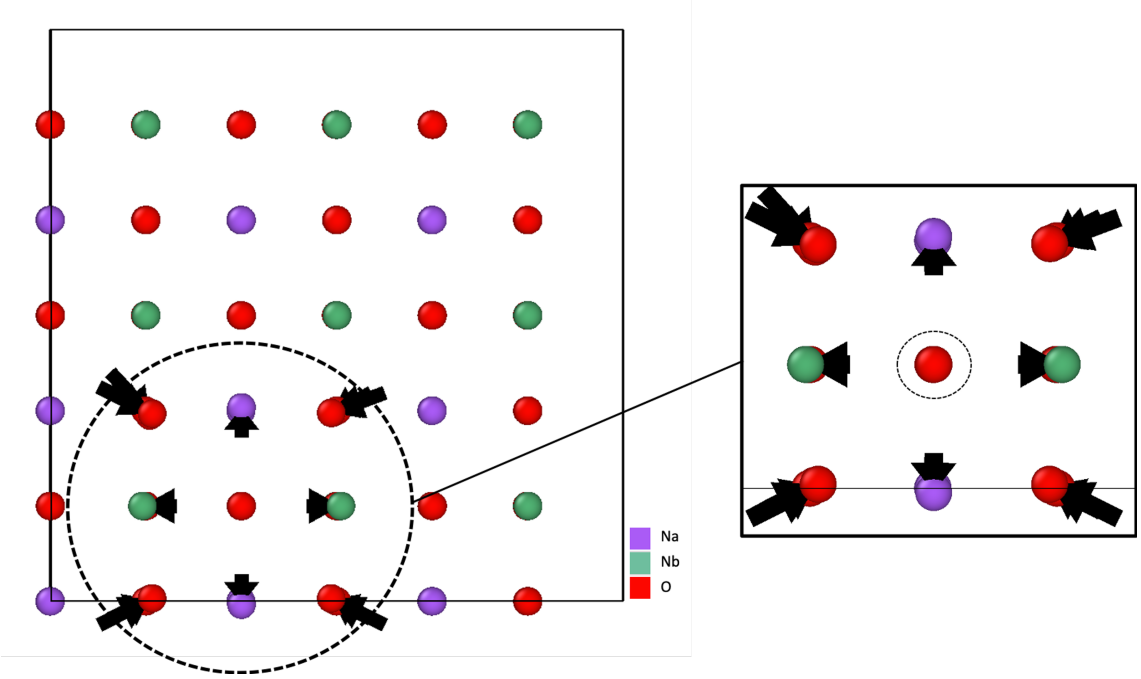

Figure 5.11: Applied manual distortion on relaxed pure structure of 3×3×3 supercell of cubic $NaNbO_3$*. Oxygen atoms are displaced by 0.1 Å inward toward O atom in the center, Nb and Na atoms are displaced further away from O atom in the center.*

The manually distorted supercell is then used as the initial configuration for investigation of polaron in this phase. One electron is removed from the system and U parameter of 4 eV on Nb(4d) states and U parameter of 2, 4, 6, 8, 10, and 12 eV is applied on O(2p) states. For U parameters of 2, 10, and 12 eV on O(2p) states no polaron is observed. Fig.5.12 shows the distribution of charge on different atoms in distorted and ideal structure of cubic $NaNbO_3$. Fig. 5.12.a shows that since there is no distortion in the system, the excess positive charge is almost equally distributed over all the O atoms in the system while Fig. 5.12.b shows that charge is majorly localized on a single O atom (on 2p orbital). O atoms around the one with polaron, have higher charge localization compared to all the other O atoms in the system.

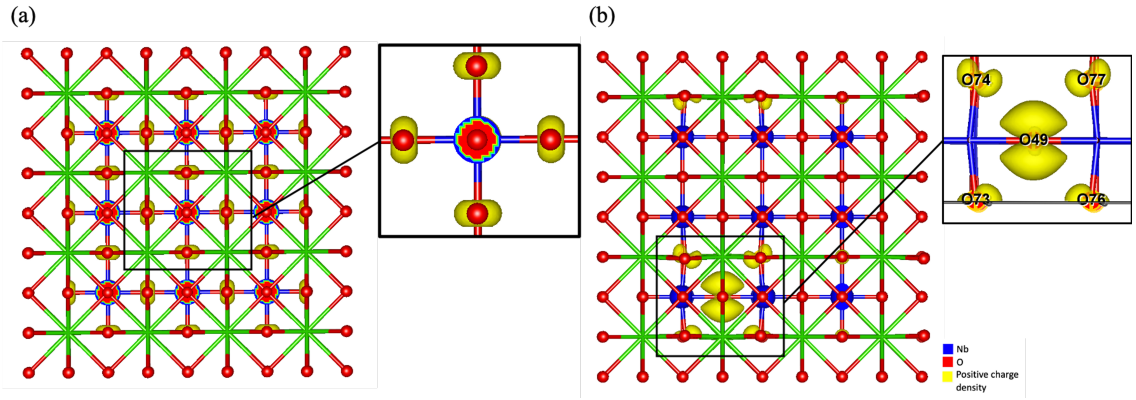

Figure 5.12: Schematic illustration of partial charge density in (a) pure structure, and (b) polaronic configuration of cubic $NaNbO_3$.

Fig. 5.13 shows how atoms are displaced through relaxation after application of manual distortion and removal of one electron from the system. Table 5.5 shows the value for displacements of O atom having the polaron (which charge is mainly localized on it) and its neighboring O atoms. Compared to rhombohedral phase, neighbouring O atoms have higher displacement and polarisation. The O atom which polaron is formed on its 2p orbital is number 103. As shown in the table 5.5, the magnetization of this O (number 103) is 0.728 which clearly indicates that charge is mainly localized on this site and the rest of the charge is distributed over O atoms in its vicinity. Charge density on the rest of the O atoms in the system is in the range of 0.000-0.003 eV. Based on the displacements in Fig. 5.13, the O atoms around polaronic site are moved closer to the O atom in the center. Reported displacements and magnetization belong to the configuration where U parameter of 4 and 8 eV is applied on Nb(4d) and O(2p) states, respectively.

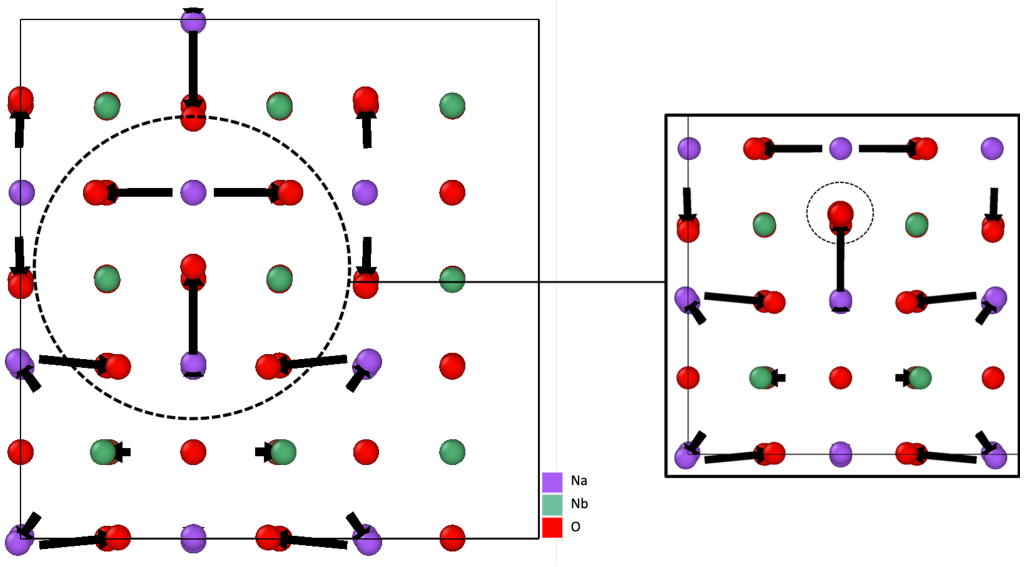

Figure 5.13: Schematic illustration of displacement of atoms after relaxation of ideal supercell with one excess positive charge and manual distortion in the 3×3×3 supercell of cubic $NaNbO_3$*; O atoms around the O atom in the center where polaron is formed (the one which is circumvented by a dashed line) are displaced significantly.*

Table 5.5: Displacements and magnetization of O atoms in the polaronic site in the 3×3×3 supercell of cubic $NaNbO_3$*.*

Atom type	Number	Displacement [Å]	Magnetisation
O	103	0.29147	0.728
O	127	+0.263331	0.07
O	128	-0.25351	0.07
O	130	+0.262393	0.07
O	131	-0.253452	0.07

Fig. 5.14 indicates PDOS and BS of 3×3×3 cubic supercell of $NaNbO_3$ where STH band state is clearly shown for application of DFT+U with various U parameters on O(2p) states. Fig. 5.14.a and b show PDOS and BS of systems which U(Nb4d)=4 eV and U(O2p)=4 eV, respectively. Fig. 5.14.c and d show same plots for U parameter of 4 eV on Nb(4d) states and U parameter of 6 on O(2p) states. In Fig. 5.14.e and f, the U parameter on Nb(4d) states is again kept constant on 4 eV while U parameter on O(2p) states is increased to 8 eV. PDOS and BS for a configuration where U parameter of 4 eV on Nb(4d) and U parameter of 10 eV on O(2p) states is shown in Fig. 5.14.g and f. The applied manual distortion (shown in Fig. 5.11) plus removal of one electron from the system has lead to the formation of a polaronic state in 3×3×3 supercell of cubic $NaNbO_3$. Regarding U parameter of 2 eV on O(2p) states no polaron is formed, since this U value is too small for maintaining a charge in a localized state.

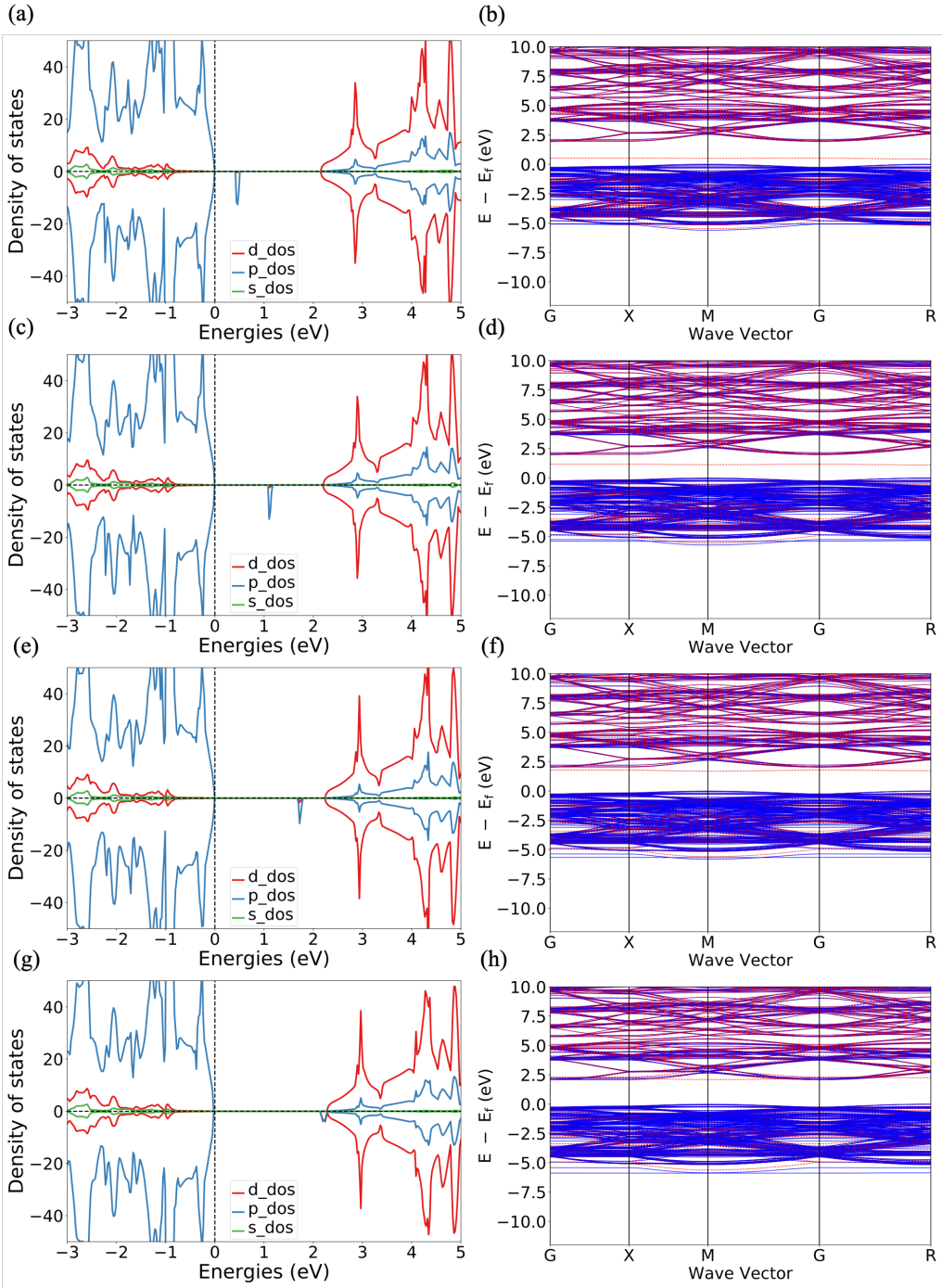

Figure 5.14: Partial density of states (PDOS) and band structures (BS) obtained by applying U parameter of 4 eV on Nb(4d) states and different U parameters on O(2p) states; (a) PDOS for U=4 eV on O(2p) states, (b) BS for U=4 eV on O(2p) states, (c) PDOS for U=6 eV on O(2p) states, (d) BS for U=6 eV on O(2p) states, (e) PDOS for U=8 eV on O(2p) states, (f) BS for U=8 eV on O(2p) states, and (g) PDOS for U=10 eV on O(2p) states, (h) BS for U=10 eV on O(2p) states.

Position of STH band level with repect to VBM is shown in table 5.5. Similar to the results obtained for the rhombohedral phase, increasing the U parameter cause

the band level to move further away from VBM. By going through the value of magnetization for the atoms in the polaronic site (close to O with number 103), it is clearly observed that the charge is mainly localized on single O atom and localization increases by increasing the U parameter from 4 to 8 eV. Similar to rhombohedral phase, increasing the U parameter moves the STH level closer to CBM.

Table 5.6: STH band level with respect to VBM, total magnetization and magnetization on O atom number 103 for various U parameters on O(2p) states in 3×3×3 supercell of cubic $NaNbO_3$.

U (O2p) [eV]	U(Nb4d) [eV]	STH level with respect to VBM	Total Magnetisation	Magnetisation on O (atom 103)
4	4	0.45	0.873	0.569
4	6	1.07	0.877	0.673
4	8	1.71	0.880	0.728
4	10	2.21	0.882	0.762

5.2.3 Polaron energy regimes and configuration coordinate diagram

Table 5.7 shows the calculated formation energy based on equation 5.1 and equation 5.4. U parameter of 4 eV on O(2p) leads to a positive formation energy from both equations which can be interpreted as such polaron in the structure is in a metastable state. Similar to obtained results from rhombohedral phase of $NaNbO_3$, trapping energy noticeably increases as the U parameter on O(2p) increases which was expected. By increasing the U parameter, the excess charge becomes more bound to the polaronic site and trapping energy increases. Comparing the trapping energy obtained from equation 5.1 and formation energy acquired from equation 5.4, shows that the difference is somehow noticeable and choice of 2×2×2 as k-points grid may not be the good option. In order to have a better accuracy on polaron energy regimes, a convergence test on k-points grid needs to be done.

Table 5.7: Polaron energy regimes for various U parameters in 3×3×3 supercell of cubic $NaNbO_3$.

U (Nb4d) [eV]	4	4	4
U (O2p) [eV]	4	6	8
Trapping Energy [eV]	+0.09	-0.13	-0.39
Strain Energy [eV]	+0.03	+0.04	+0.06
Electronic energy [eV]	+0.06	-0.17	-0.46
Formation Energy based on Eq. 5.4 [eV]	+0.01	-0.21	-0.55

Fig. 5.15 shows configuration coordinate diagram of a configuration where U parameter of 4 eV and 6 eV is applied on Nb(4d) and O(2p) states, respectively. Comparing this diagram with the one belongs to rhombohedral phase (Fig. 5.6) where in both the same composition of U parameter is applied on Nb and O, indicates that the polaronic state in rhombohedral phase is significantly more stable than the polaron in the cubic phase. Trapping energy for application of U(Nb4d)=4 eV and U(O2p)=6 eV in cubic and rhombohedral phase of $NaNbO_3$ are -0.13 and -0.38 eV, respectively.

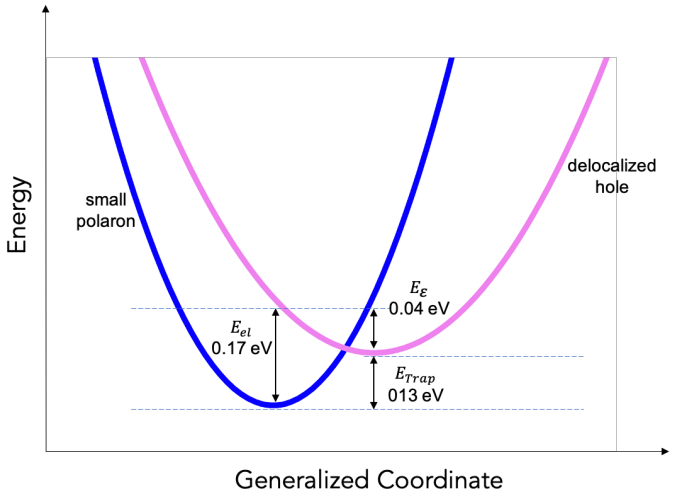

Figure 5.15: Configuration coordinate diagram for formation of stable small polaron in 3×3×3 distorted supercell of cubic $NaNbO_3$ *by applying U parameter of 4 eV on Nb(4d) states and U parameter of 6 eV on O(2p) states.*

5.2.4 Piecewise linearity diagrams

Fig.5.17 shows variation of the total energy with respect to fractional charge by applying various U parameters on Nb(4d) and O(2p) states, simultaneously. In all the plots, U parameter on Nb(4d) states is kept constant with 4, 6, 8 eV while the U parameter on O(2p) states is changing between 2, 4, 6, 8, 10, and 12 eV. For the U parameter of 4 eV on Nb(4d) states, the optimum U parameter which shows a better piecewise linear behavior are 2, 4, and 6 eV, respectively. For U parameter of 6 eV on Nb, U parameters of 2, 4, and 6 eV are optimum U values on O(2p) states. For the U parameter of 8 eV on Nb, similar results as U parameter of 4 eV on Nb is obtained.

Fig. 5.16 shows all the good options of the U parameters applied on Nb and O (Fig. 5.16) which can be beneficial for choosing the final value. The following composition of U on Nb and O:

- U(Nb4d)=8 eV, U(O2p)=2 eV
- U(Nb4d)=6 eV, U(O2p)=6 eV

show better linear behavior compared to others. At this stage, it is also advantageous to compare the lattice parameters of the current systems with the available experimental data.

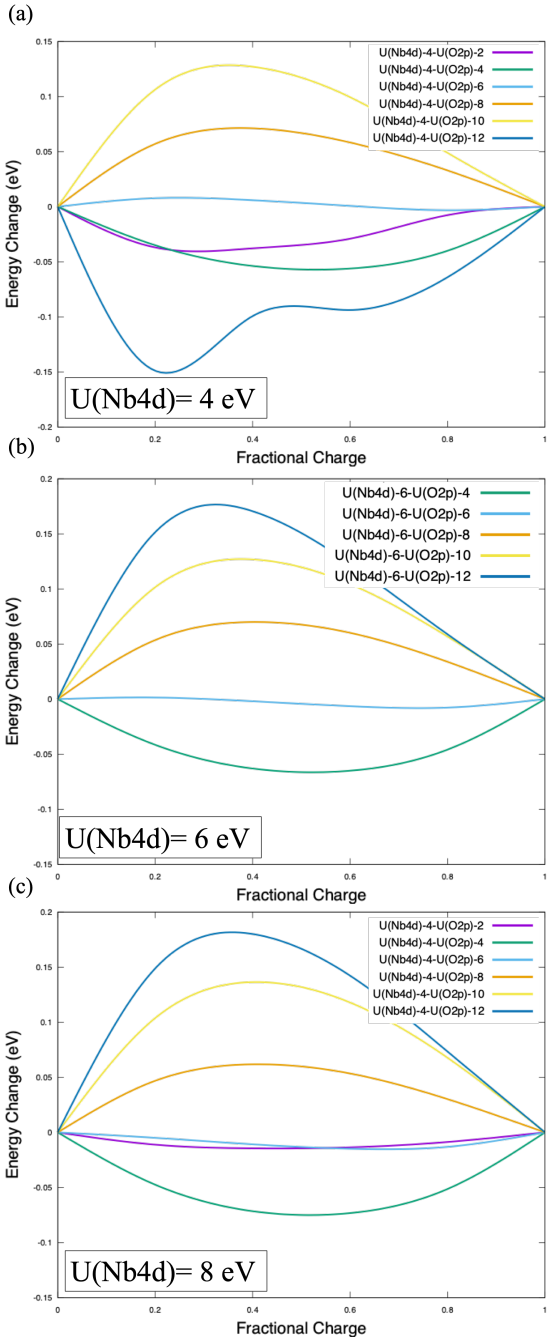

Figure 5.17: Application of various U parameters on Nb(4d) and O(2p) states simultaneously, using the polaronic configuration as the initial structure in the 3×3×3 supercell of cubic $NaNbO_3$*.]*

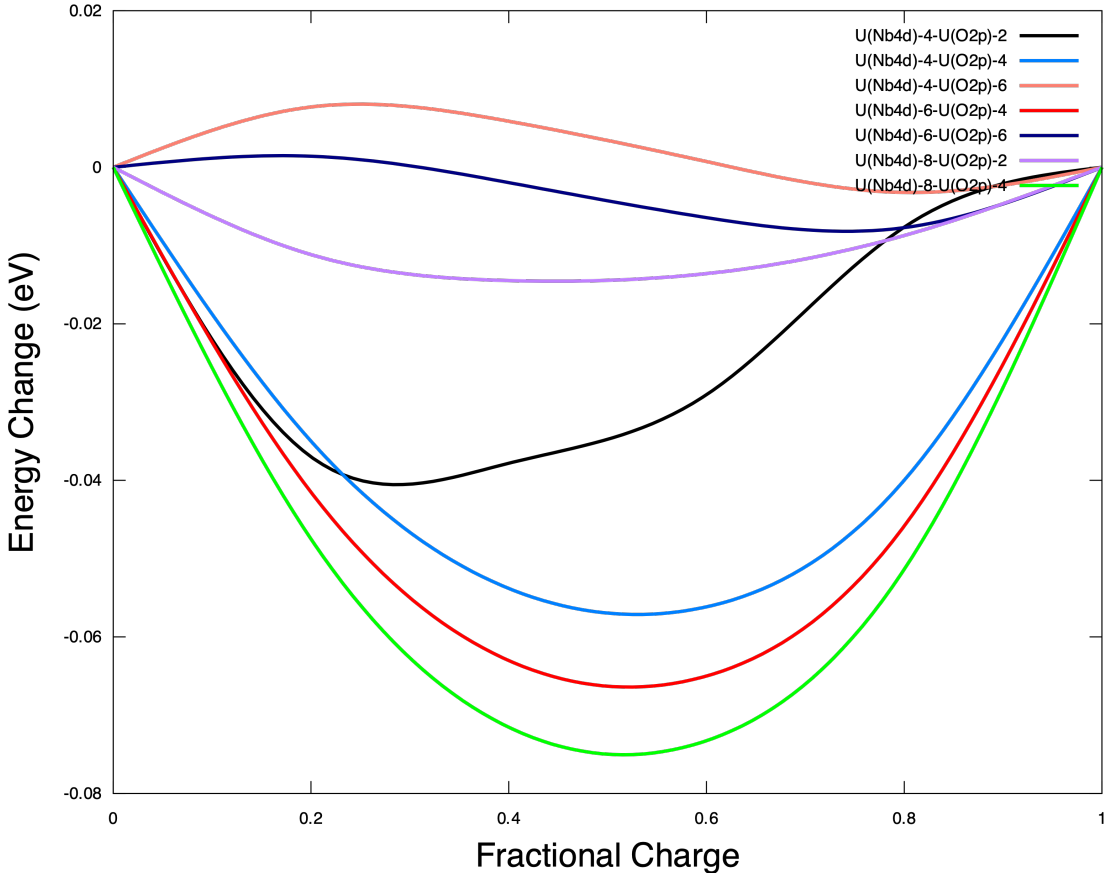

Figure 5.16: Comparison of piecewise linearity behavior of the total energy with respect to the fractional charge of 3×3×3 supercell of the cubic $NaNbO_3$ *by applying different U parameters on both Nb(4d) and O(2p) states using polaronic configuration as the initial system.*

Table 5.8 shows lattice parameters of cubic $NaNbO_3$ using PBE and PBEsol functional. As already stated by Fritsch et al. [12] lattice parameter values obtained from PBEsol are closer to the experimental value of 3.95 Å. By comparing lattice parameters obtained using PBE and PBEsol in the systems with different U parameters and considering the very good linear behavior of a wide range of U parameters, both:

- U(Nb4d)=4 eV, U(O2p)=4 eV,
- U(Nb4d)=4 eV, U(O2p)=6 eV,

can be acceptable options. However, the first composition leads to a positive trapping energy and metastable polaronic state. Although, DFT+U can slightly reduce the band gap error of DFT, however, as it can be seen in the table 5.8, the band gap of cubic system is significantly underestimated compared to the experimental value of 3.29 eV (which this was not the case for rhombohedral phase). Although increasing the U parameter may lead to a better estimation for band energy of the system as it covers for over-delocalization of DFT method, the piecewise linear behavior of the total energy with respect to fractional charge is less reliable using high

unrealistic U parameter on the atomic orbitals.

Table 5.8: Lattice parameters and energy band gap obtained using PBE and PBEsol in 3×3×3 supercell of cubic $NaNbO_3$.

U(Nb4d) [eV]	U(O2p) [eV]	Existence of Polaron	Lattice Parameter [Å] (PBEsol-unitcell)	Lattice Parameter [Å] (PBE-supercell)	Band Gap [eV] (PBE)	Band Gap [eV] (PBEsol)
4	2	No	3.970	3.993	2.12	2.11
4	4	Yes	3.966	3.991	2.18	2.16
4	6	Yes	3.962	3.982	2.23	2.21
4	8	Yes	3.957	3.982	2.29	2.26
4	10	No	3.952	3.977	2.35	2.32
4	12	No	3.946	3.971	2.42	2.38
6	2	No	3.984	4.008	2,41	2.38
6	4	Yes	3.980	4.005	2.46	2.44
6	6	Yes	3.975	4.003	2.51	2.50
6	8	Yes	3.970	3.995	2.58	2.56
6	10	No	3.965	3.990	2.65	2.62
6	12	No	3.960	3.985	2.73	2.69
8	2	No	4.002	4.023	2.68	2.65
8	4	No	3.994	4.019	2.74	2.72
8	6	Yes	3.989	4.014	2.81	2.78
8	8	Yes	3.984	4.008	2.88	2.85
8	10	Yes	3.979	4.005	2.95	2.92
8	12	No	3.973	4.002	3.02	3.00

Chapter 6

Conclusion and outlook

In summary, we have demonstrated that application a manual distortion in the lattice structure along with removal of one charge at both low and high temperature phases of $NaNbO_3$, can encourage the formation of small polarons in the system using both HSE06 and PBE+U functionals. Simulations has shown that increasing the U parameter on O, can significantly increase the trapping energy of STH which is due to the fact that addition of Hubbard U parameter will cancel out the self-interaction error of DFT and successfullly localise the charges at the site of distortion. However, application of U parameter separately on O(2p) states has shown that increasing the U parameter cause large deviation from piecewise linear behaviour. Consequently, U parameters larger than 6 eV are not considered as a good option for U value on O since it only consists of s and p orbitals.

Comparing different energy regimes of cubic and rhombohedral phases show that rhombohedral phase has higher gain in energy compared to the cubic phase for the same value of U parameter on Nb and O which leads to the fact that STH polarons are more probable to be observed in the rhombohedral phase of $NaNbO_3$ through experimental studies. Various compositions of U parameter on Nb and O have shown a good agreement with piecewise linearity of total energy versus fractional charge.

In order to choose the optimum value of U for application on Nb and O atoms, the piecewise linear behavior of a system which the composition of U parameter on both Nb and O is applied, has been investigated by plotting the total energy versus fractional charge density. In order to narrow down the available options which are all in good agreement with piecewise linearity method, other properties of each system such as lattice parameters and band gap is also investigated using PBE and PBEsol. For rhombohedral phase of $NaNbO_3$, choice of U(Nb4d)= 4,6 eV and U(O2p)=4 eV have a good agreement with experimental data. For cubic phase, U(Nb4d)= 4 eV and U(O2p)= 6 eV is the best choice of U value which yields a good picewise linear behavior along with more precise prediction of lattice parameters.

In this work, formation of polaron in both cubic and rhombohedral phases is confirmed while the optimum value of U parameter is chosen by precise comparsion

between polaronic energy regimes. Our proposed scheme for continuing this research would be the use of Occupation Matrix Control (OMC) in order to place the polaron without manually distorting the lattice and more flexibility in choosing the polaronic site. Using OMC can pave the way for investigation of hopping energy using Nudge Elastic Band (NEB) method as by specifying two neighbouring sites which polaron can move between them, the activation energy barrier for hopping mechanism can be calculated. Having access to hopping energy barrier of polaron in $NaNbO_3$ is very important because it is one of the decisive factors regarding the mobility of charges in the system. Due to the time limitation, this study is only done for a supercell system of $2\times2\times3$ for the rhombohedral phase and $3\times3\times3$ for cubic phase. Interesting result is expected by doing finite size correction.

Bibliography

[1] Jozef T. Devreese. More on polaron theory history. *Physics Today*, 68(9):11–11, August 2015. Publisher: American Institute of Physics.

[2] L. D. Landau. Über Die Bewegung der Elektronen in Kristallgitter. *Phys.Z.Sowjetunion*, 3:644–645, 1933.

[3] David Emin. Optical properties of large and small polarons and bipolarons. *Physical Review B*, 48(18):13691–13702, November 1993. Publisher: American Physical Society.

[4] Nevill Francis Mott and Edward A. Davis. *Electronic Processes in Non-Crystalline Materials*. Oxford Classic Texts in the Physical Sciences. Oxford University Press, Oxford, New York, February 2012.

[5] Yuriy Natanzon, Amram Azulay, and Yaron Amouyal. Evaluation of Polaron Transport in Solids from First-principles. *Israel Journal of Chemistry*, n/a(n/a). _eprint: https://onlinelibrary.wiley.com/doi/pdf/10.1002/ijch.201900101.

[6] Paul Erhart, Andreas Klein, Daniel Åberg, and Babak Sadigh. Efficacy of the DFT + U formalism for modeling hole polarons in perovskite oxides. *Physical Review B*, 90(3):035204, July 2014. Publisher: American Physical Society.

[7] A. J. Nozik. Photochemical diodes. *Applied Physics Letters*, 30(11):567–569, June 1977. Publisher: American Institute of Physics.

[8] Jiajun Wang, Jing Teng, Lizhi Pu, Jing Huang, Ying Wang, and Qunxiang Li. Double-hole-mediated coupling of anionic dopants in perovskite NaNbO3 for efficient solar water splitting. *International Journal of Quantum Chemistry*, 119(14):e25930, 2019. _eprint: https://onlinelibrary.wiley.com/doi/pdf/10.1002/qua.25930.

[9] Hideki Kato, Kiyotaka Asakura, and Akihiko Kudo. Highly Efficient Water Splitting into H2 and O2 over Lanthanum-Doped NaTaO3 Photocatalysts with High Crystallinity and Surface Nanostructure. *Journal of the American Chemical Society*, 125(10):3082–3089, March 2003. Publisher: American Chemical Society.

[10] Xubiao Luo and Fang Deng. *Nanomaterials for the Removal of Pollutants and Resource Reutilization*. Elsevier, November 2018. Google-Books-ID: VqR6DwAAQBAJ.

[11] Helen D. Megaw. The seven phases of sodium niobate. *Ferroelectrics*, 7(1):87–89, January 1974. Publisher: Taylor & Francis _eprint: https://doi.org/10.1080/00150197408237956.

[12] Daniel Fritsch. Electronic and Optical Properties of Sodium Niobate: A Density Functional Theory Study, 2018. ISSN: 1687-8434 Library Catalog: www.hindawi.com Pages: e6416057 Publisher: Hindawi Volume: 2018.

[13] C. N. W. Darlington and H. D. Megaw. The low-temperature phase transition of sodium niobate and the structure of the low-temperature phase, N. *Acta Crystallographica Section B*, 29(10):2171–2185, 1973. _eprint: https://onlinelibrary.wiley.com/doi/pdf/10.1107/S0567740873006308.

[14] C. I. Cheon, H. W. Joo, K. W. Chae, J. S. Kim, S. H. Lee, S. Torii, and T. Kamiyama. Monoclinic ferroelectric NaNbO3 at room temperature: Crystal structure solved by using super high resolution neutron powder diffraction. *Materials Letters*, 156:214–219, October 2015.

[15] Jiaming Ye, Genshui Wang, Mingxing Zhou, Ningtao Liu, Xuefeng Chen, Song Li, Fei Cao, and Xianlin Dong. Excellent comprehensive energy storage properties of novel lead-free NaNbO3-based ceramics for dielectric capacitor applications. *Journal of Materials Chemistry C*, 7(19):5639–5645, May 2019. Publisher: The Royal Society of Chemistry.

[16] Zhonghua Yao, Zhe Song, Hua Hao, Zhiyong Yu, Minghe Cao, Shujun Zhang, Michael T. Lanagan, and Hanxing Liu. Homogeneous/Inhomogeneous-Structured Dielectrics and their Energy-Storage Performances. *Advanced Materials*, 29(20):1601727, 2017. _eprint: https://onlinelibrary.wiley.com/doi/pdf/10.1002/adma.201601727.

[17] Qi Li, Fang Zhou Yao, Yang Liu, Guangzu Zhang, Hong Wang, and Qing Wang. High-Temperature Dielectric Materials for Electrical Energy Storage. *Annual Review of Materials Research*, 48:219–243, July 2018. Publisher: Annual Reviews Inc.

[18] Grégory Geneste, Bernard Amadon, Marc Torrent, and Guilhem Dezanneau. DFT+U study of self-trapping, trapping, and mobility of oxygen-type hole polarons in barium stannate. *Physical Review B*, 96(13):134123, October 2017. Publisher: American Physical Society.

[19] O. F. Schirmer. Holes bound as small polarons to acceptor defects in oxide materials: why are their thermal ionization energies so high? *Journal of Physics. Condensed Matter: An Institute of Physics Journal*, 23(33):334218, August 2011.

[20] A. J. Fisher, W. Hayes, and D. S. Wallace. Polarons and solitons. *Journal of Physics: Condensed Matter*, 1(33):5567–5593, August 1989. Publisher: IOP Publishing.

[21] H. Fröhlich. Electrons in lattice fields. *Advances in Physics*, 3(11):325–361, July 1954. Publisher: Taylor & Francis _eprint: https://doi.org/10.1080/00018735400101213.

[22] Steffen Richter, Oliver Herrfurth, Shirly Espinoza, Mateusz Rebarz, Miroslav Kloz, Joshua A. Leveillee, André Schleife, Stefan Zollner, Marius Grundmann, Jakob Andreasson, and Rüdiger Schmidt-Grund. Ultrafast dynamics of hot charge carriers in an oxide semiconductor probed by femtosecond spectroscopic ellipsometry. *arXiv:1902.05832 [cond-mat]*, November 2019. arXiv: 1902.05832.

[23] Lior Kornblum. Conductive Oxide Interfaces for Field Effect Devices. *Advanced Materials Interfaces*, 6(15):1900480, 2019. _eprint: https://onlinelibrary.wiley.com/doi/pdf/10.1002/admi.201900480.

[24] Divine P. Kumah, Joseph H. Ngai, and Lior Kornblum. Epitaxial Oxides on Semiconductors: From Fundamentals to New Devices. *Advanced Functional Materials*, 30(18):1901597, 2020. _eprint: https://onlinelibrary.wiley.com/doi/pdf/10.1002/adfm.201901597.

[25] Xing Tan, Jin-Le Lan, Yao-Chun Liu, Guang-Kun Ren, Cheng-Cheng Zeng, Yuan-Hua Lin, and Cewen Nan. Optimization of the thermoelectric properties of Bi2O2Se ceramics by altering the temperature of spark plasma sintering. *Journal of Electroceramics*, 37(1):66–72, December 2016.

[26] J. Bonča, S. A. Trugman, and I. Batistić. Holstein polaron. *Physical Review B*, 60(3):1633–1642, July 1999. Publisher: American Physical Society.

[27] Kiyoshi Miyata, Daniele Meggiolaro, M. Tuan Trinh, Prakriti P. Joshi, Edoardo Mosconi, Skyler C. Jones, Filippo De Angelis, and X.-Y. Zhu. Large polarons in lead halide perovskites. *Science Advances*, 3(8):e1701217, August 2017. Publisher: American Association for the Advancement of Science Section: Research Article.

[28] Julius Ranninger. Introduction to polaron physics: Basic Concepts and Models. *arXiv:cond-mat/0606665*, June 2006. arXiv: cond-mat/0606665.

[29] null Jaime, null Salamon, null Rubinstein, null Treece, null Horwitz, and null Chrisey. High-temperature thermopower in La2/3Ca1/3MnO3 films: Evidence for polaronic transport. *Physical Review. B, Condensed Matter*, 54(17):11914–11917, November 1996.

[30] Guoqing Wu and J. J. Neumeier. Small polaron transport and pressure dependence of the electrical resistivity of ${\mathrm{La}}_{2\ensuremath{-}x}{\mathrm{Sr}}_{x}{\mathrm{NiO}}_{4}(0<~x<~1.2)$. *Physical Review B*, 67(12):125116, March 2003. Publisher: American Physical Society.

[31] Helen D. Megaw. The seven phases of sodium niobate. *Ferroelectrics*, 7(1):87–89, January 1974. Publisher: Taylor & Francis _eprint: https://doi.org/10.1080/00150197408237956.

[32] Yosuke Shiratori, Arnaud Magrez, Werner Fischer, Christian Pithan, and Rainer Waser. Temperature-induced Phase Transitions in Micro-, Submicro-

, and Nanocrystalline NaNbO3. *The Journal of Physical Chemistry C*, 111(50):18493–18502, December 2007. Publisher: American Chemical Society.

[33] S. K. Mishra, N. Choudhury, S. L. Chaplot, P. S. R. Krishna, and R. Mittal. Competing antiferroelectric and ferroelectric interactions in $\mathrm{Na}\mathrm{Nb}{\mathrm{O}}_{3}$: Neutron diffraction and theoretical studies. *Physical Review B*, 76(2):024110, July 2007. Publisher: American Physical Society.

[34] S. K. Mishra, R. Mittal, V. Yu. Pomjakushin, and S. L. Chaplot. Phase stability and structural temperature dependence in sodium niobate: A high-resolution powder neutron diffraction study. *Physical Review B*, 83(13):134105, April 2011. Publisher: American Physical Society.

[35] Daniel Fritsch. Electronic and Optical Properties of Sodium Niobate: A Density Functional Theory Study. *Advances in Materials Science and Engineering*, 2018:1–9, 2018.

[36] A. C. Sakowski-Cowley, K. Łukaszewicz, and H. D. Megaw. The structure of sodium niobate at room temperature, and the problem of reliability in pseudosymmetric structures. *Acta Crystallographica Section B*, 25(5):851–865, 1969. _eprint: https://onlinelibrary.wiley.com/doi/pdf/10.1107/S0567740869003141.

[37] Karen E. Johnston, Chiu C. Tang, Julia E. Parker, Kevin S. Knight, Philip Lightfoot, and Sharon E. Ashbrook. The polar phase of NaNbO(3): a combined study by powder diffraction, solid-state NMR, and first-principles calculations. *Journal of the American Chemical Society*, 132(25):8732–8746, June 2010.

[38] M. Boukriba, F. Sediri, and N. Gharbi. Hydrothermal synthesis and electrical properties of NaNbO3. *Materials Research Bulletin*, 48(2):574–580, February 2013.

[39] H. Englisch, H. Fieseler, and A. Haufe. Density-functional calculations for excited-state energies. *Physical Review A*, 37(12):4570–4576, June 1988. Publisher: American Physical Society.

[40] Jean-Luc Fattebert and François Gygi. Density functional theory for efficient ab initio molecular dynamics simulations in solution. *Journal of Computational Chemistry*, 23(6):662–666, 2002. _eprint: https://onlinelibrary.wiley.com/doi/pdf/10.1002/jcc.10069.

[41] A. K. Rajagopal. Theory of Inhomogeneous Electron Systems: Spin-Density-Functional Formalism. In *Advances in Chemical Physics*, pages 59–193. John Wiley & Sons, Ltd, 2007. _eprint: https://onlinelibrary.wiley.com/doi/pdf/10.1002/9780470142608.ch2.

[42] J. Harris and R. O. Jones. Pseudopotentials in Density-Functional Theory. *Physical Review Letters*, 41(3):191–194, July 1978. Publisher: American Physical Society.

[43] Erich Runge and E. K. U. Gross. Density-Functional Theory for Time-Dependent Systems. *Physical Review Letters*, 52(12):997–1000, March 1984. Publisher: American Physical Society.

[44] W. Kohn and L. J. Sham. Self-Consistent Equations Including Exchange and Correlation Effects. *Physical Review*, 140(4A):A1133–A1138, November 1965. Publisher: American Physical Society.

[45] Andreas Görling. Density-functional theory beyond the Hohenberg-Kohn theorem. *Physical Review A*, 59(5):3359–3374, May 1999. Publisher: American Physical Society.

[46] Stefan Grimme and Mirko Waletzke. A combination of Kohn–Sham density functional theory and multi-reference configuration interaction methods. *The Journal of Chemical Physics*, 111(13):5645–5655, September 1999. Publisher: American Institute of Physics.

[47] A. Seidl, A. Görling, P. Vogl, J. A. Majewski, and M. Levy. Generalized Kohn-Sham schemes and the band-gap problem. *Physical Review B*, 53(7):3764–3774, February 1996. Publisher: American Physical Society.

[48] null Yabana and null Bertsch. Time-dependent local-density approximation in real time. *Physical Review. B, Condensed Matter*, 54(7):4484–4487, August 1996.

[49] Kieron Burke, John P. Perdew, and Yue Wang. Derivation of a Generalized Gradient Approximation: The PW91 Density Functional. In John F. Dobson, Giovanni Vignale, and Mukunda P. Das, editors, *Electronic Density Functional Theory: Recent Progress and New Directions*, pages 81–111. Springer US, Boston, MA, 1998.

[50] John P. Perdew, Kieron Burke, and Matthias Ernzerhof. Generalized Gradient Approximation Made Simple. *Physical Review Letters*, 77(18):3865–3868, October 1996. Publisher: American Physical Society.

[51] A Chemist's Guide to Density Functional Theory | Wiley Online Books.

[52] Ann E. Mattsson, Peter A. Schultz, Michael P. Desjarlais, Thomas R. Mattsson, and Kevin Leung. Designing meaningful density functional theory calculations in materials science—a primer. *Modelling and Simulation in Materials Science and Engineering*, 13(1):R1–R31, November 2004. Publisher: IOP Publishing.

[53] Eugene S. Kryachko. Density Functional Theory and Molecular Interactions: Dispersion Interactions. In Mihai V. Putz and D. Michael P. Mingos, editors, *Applications of Density Functional Theory to Biological and Bioinorganic Chemistry*, Structure and Bonding, pages 65–96. Springer, Berlin, Heidelberg, 2013.

[54] B. H. Brandow. Theory of mott insulators. *International Journal of Quantum Chemistry*, 10(S10):417–434, 1976. _eprint: https://onlinelibrary.wiley.com/doi/pdf/10.1002/qua.560100845.

[55] Burak Himmetoglu, Andrea Floris, Stefano de Gironcoli, and Matteo Cococcioni. Hubbard-corrected DFT energy functionals: The LDA+U description of correlated systems. *International Journal of Quantum Chemistry*, 114(1):14–49, 2014. _eprint: https://onlinelibrary.wiley.com/doi/pdf/10.1002/qua.24521.

[56] Matteo Cococcioni. The LDA + U Approach : A Simple Hubbard Correction for Correlated Ground States. 2012.

[57] Henrik Bruus and Karsten Flensberg. *Many-Body Quantum Theory in Condensed Matter Physics: An Introduction*. Oxford University Press, Oxford ; New York, November 2004.

[58] Sarah A. Tolba, Kareem M. Gameel, Basant A. Ali, Hossam A. Almossalami, and Nageh K. Allam. The DFT+U: Approaches, Accuracy, and Applications. *Density Functional Calculations - Recent Progresses of Theory and Application*, May 2018. Publisher: IntechOpen.

[59] Fabien Tran, Peter Blaha, Karlheinz Schwarz, and Pavel Novák. Hybrid exchange-correlation energy functionals for strongly correlated electrons: Applications to transition-metal monoxides. *Physical Review B*, 74(15):155108, October 2006. Publisher: American Physical Society.

[60] Eli Kraisler and Leeor Kronik. Piecewise Linearity of Approximate Density Functionals Revisited: Implications for Frontier Orbital Energies. *Physical Review Letters*, 110(12):126403, March 2013. arXiv: 1211.5950.

[61] D. I. Bilc, R. Orlando, R. Shaltaf, G.-M. Rignanese, Jorge Íñiguez, and Ph. Ghosez. Hybrid exchange-correlation functional for accurate prediction of the electronic and structural properties of ferroelectric oxides. *Physical Review B*, 77(16):165107, April 2008. Publisher: American Physical Society.

[62] A. M. Stoneham, J. Gavartin, A. L. Shluger, A. V. Kimmel, D. Muñoz Ramo, H. M. Rønnow, G. Aeppli, and C. Renner. Trapping, self-trapping and the polaron family. *Journal of Physics: Condensed Matter*, 19(25):255208, May 2007. Publisher: IOP Publishing.

[63] Michele Reticcioli, Ulrike Diebold, Georg Kresse, and Cesare Franchini. Small Polarons in Transition Metal Oxides. *arXiv:1902.04183 [cond-mat]*, pages 1–39, 2019. arXiv: 1902.04183.